AD-A162 192

(2)

AFGL-TR-85-0133
ENVIRONMENTAL RESEARCH PAPERS, NO. 922

# Vibro-Acoustic Forecasts for STS Launches at V23, Vandenberg AFB: Results Summary and the Payload Preparation Room


JAMES CRAIG BATTIS




8 May 1985






EARTH SCIENCES DIVISION PROJECT 7600

AIR FORCE GEOPHYSICS LABORATORY

HANSCOM AFB, MA 01731

# DISCLAIMER NOTICE

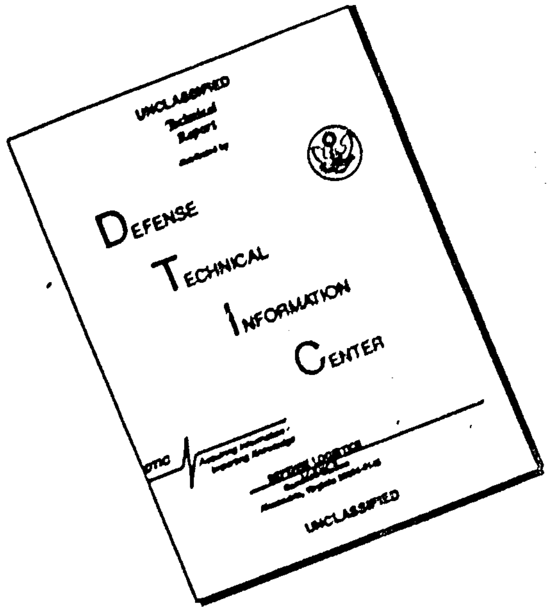


THIS DOCUMENT IS BEST QUALITY AVAILABLE. THE COPY FURNISHED TO DTIC CONTAINED A SIGNIFICANT NUMBER OF PAGES WHICH DO NOT REPRODUCE LEGIBLY.

## IN-HOUSE REPORTS

This technical report has been reviewed and is approved for publication.

FOR THE COMMANDER

HENRY A. OSSING
Chief, Solid Earth Geophysics Branch

DONALD H. ECKHARDT
Director
Earth Sciences Division

This document has been reviewed by the ESD Public Affairs Office (PA) and is releasable to the National Technical Information Service (NTIS).

Qualified requestors may obtain additional copies from the Defense Technical Information Center. All others should apply to the National Technical Information Service.

If your address has changed, or if you wish to be removed from the mailing list, or if the addressee is no longer employed by your organization, please notify AFGL/DAA, Hanscom AFB, MA 01731. This will assist us in maintaining a current mailing list.

UNCLASSIFIED
SECURITY CLASSIFICATION OF THIS PAGE

AD-A162 192

## REPORT DOCUMENTATION PAGE

| | |
|---|---|
| 1a. REPORT SECURITY CLASSIFICATION<br>Unclassified | 1b. RESTRICTIVE MARKINGS |
| 2a. SECURITY CLASSIFICATION AUTHORITY | 3. DISTRIBUTION/AVAILABILITY OF REPORT<br>Approved for public release; distribution unlimited. |
| 2b. DECLASSIFICATION/DOWNGRADING SCHEDULE | |
| 4. PERFORMING ORGANIZATION REPORT NUMBER(S)<br>AFGL-TR-85-0133<br>ERP, No. 922 | 5. MONITORING ORGANIZATION REPORT NUMBER(S) |
| 6a. NAME OF PERFORMING ORGANIZATION<br>Air Force Geophysics Laboratory<br>6b. OFFICE SYMBOL (If applicable)<br>LWH | 7a. NAME OF MONITORING ORGANIZATION |
| 6c. ADDRESS (City, State and ZIP Code)<br>Hanscom AFB<br>Massachusetts 01731 | 7b. ADDRESS (City, State and ZIP Code) |
| 8a. NAME OF FUNDING/SPONSORING ORGANIZATION<br>8b. OFFICE SYMBOL (If applicable) | 9. PROCUREMENT INSTRUMENT IDENTIFICATION NUMBER |
| 8c. ADDRESS (City, State and ZIP Code) | 10. SOURCE OF FUNDING NOS.<br>PROGRAM ELEMENT NO.: 62101F<br>PROJECT NO.: 7600<br>TASK NO.: 09<br>WORK UNIT NO.: 05 |

11. TITLE (Include Security Classification) Vibro-Acoustic Forecasts for STS Launches at V23, Vandenberg AFB: Results Summary and the Payload Preparation Room

12. PERSONAL AUTHOR(S)
Battis, James Craig

| 13a. TYPE OF REPORT | 13b. TIME COVERED | 14. DATE OF REPORT (Yr., Mo., Day) | 15. PAGE COUNT |
|---|---|---|---|
| Scientific Interim | FROM ______ TO ______ | 1985 May 8 | 88 |

16. SUPPLEMENTARY NOTATION

| 17. COSATI CODES | | | 18. SUBJECT TERMS (Continue on reverse if necessary and identify by block number) |
|---|---|---|---|
| FIELD | GROUP | SUB. GR. | Vandenberg AFB; Motion Forecasts |
| 08 | 11 | | Vibro-Acoustics |
| 20 | 01 | | STS Launch Environment |

19. ABSTRACT (Continue on reverse if necessary and identify by block number)


The launch induced vibro-acoustic environments have been forecast for several Ground Support System structures at V23, the STS launch facility at Vandenberg AFB. These forecasts are based on site particular vibration and pressure responses determined by an explosive sounding program conducted at V23. The responses are coupled with an STS acoustic pressure term established by measurement of STS launches at KSC. This report provides a summary of the results of this effort and provides the forecasts for the vibration environment in the PPR. Motion levels in the PPR are found to be substantially below all levels of concern. However, companion studies have shown that high accelerations can be anticipated in the OFS Room and the PCR. In addition, pounding could occur between the PCR and the PPR. Strong reverberations on acoustic records from V23 indicate that launch overpressures at V23 will be significantly altered from those at KSC for the shuttle at altitude and clear of the ground. Finally, the potential of pounding due to earthquake ground motions is discussed.


| | |
|---|---|
| 20. DISTRIBUTION/AVAILABILITY OF ABSTRACT<br>UNCLASSIFIED/UNLIMITED ☒ SAME AS RPT. ☐ DTIC USERS ☐ | 21. ABSTRACT SECURITY CLASSIFICATION<br>Unclassified |
| 22a. NAME OF RESPONSIBLE INDIVIDUAL<br>James C. Battis | 22b. TELEPHONE NUMBER (Include Area Code)<br>617-861-3222<br>22c. OFFICE SYMBOL<br>LWH |

DD FORM 1473, 83 APR EDITION OF 1 JAN 73 IS OBSOLETE.

UNCLASSIFIED
SECURITY CLASSIFICATION OF THIS PAGE

# Preface

The author wishes to acknowledge the many people who contributed to the successful completion of this work. In particular, the work of Henry Ossing and A1c David Plyley of AFGL/LWH, of Francis Crowley, Eugene Hartnett, and Joseph Blaney of Boston College, of Lt Susan Ferkau of SATAF/EN and of Thomas Hancock of Martin Marietta Corp. was of inestimable value. In addition, the author also acknowledges the many people at Vandenberg AFB who contributed, in many ways, to the AFGL Sounding Program at V23.

# Contents

# Illustrations

Illustrations



# Tables

# Vibro-Acoustic Forecasts for STS Launches at V23, Vandenberg AFB: Results Summary and the Payload Preparation Room

## 1. INTRODUCTION

### 1.1 Statement of Need

During the first tens of seconds of a Space Transportation System (STS) launch at Vandenberg AFB (VAFB), Ground Support System (GSS) facilities located near the Launch Mount (LM) will be subjected to pressure and seismic loads generated by the acoustics of the Shuttle propulsion system. These dynamic loads can produce vibrations within the GSS structures that constitute potential hazards to equipment or, if sufficiently strong, threaten the mechanical integrity of the structures or their subsystems.

Therefore, there exists a compelling need to forecast the vibro-acoustic environment that will be experienced by the GSS facilities to support design and operational planning and to assist in evaluating lifetime projections for these facilities.

### 1.2 Scope of This Report

The major GSS facilities at VAFB in close proximity to the LM are shown in Figure 1. The main body of the report deals with the vibration environment forecasts for the checkout cells in the Payload Preparation Room (PPR). This

(Received for Publication 6 May 1985)

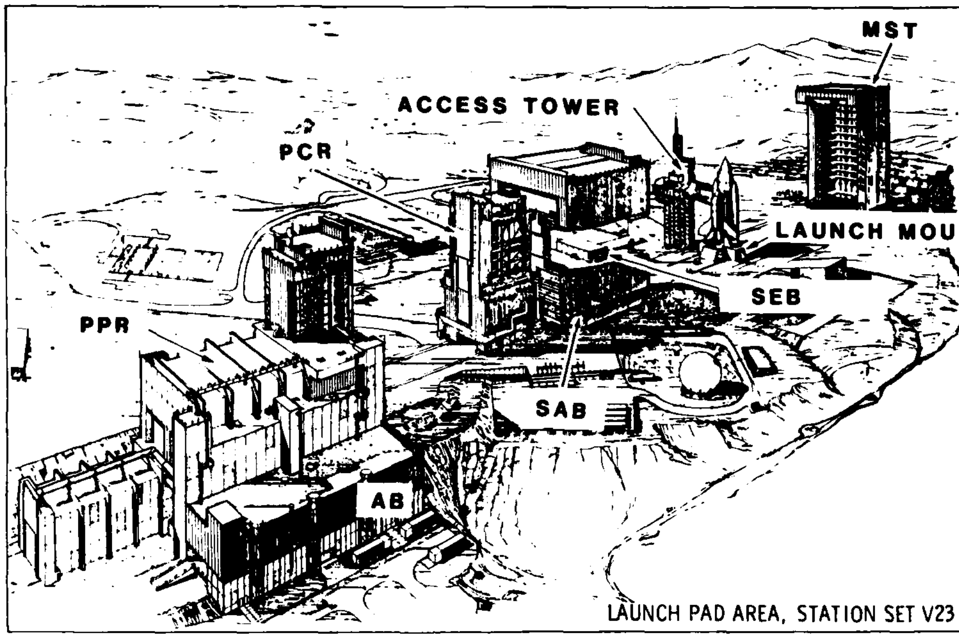


Figure 1. Major Ground Support System Structures at V23

report is the companion to a previous report providing similar vibro-acoustic forecasts for the Payload Changeout Room (PCR) and the Administration Building (AB).[1] The results of the earlier study are also abstracted in the Findings section of this report (Section 2).

### 1.3 Approach

The vibro-acoustic environment forecasts presented in this report were generated by combining an STS acoustic emissions source model with observed responses at locations on V23, the VAFB STS launch pad complex, and small explosive sources positioned along a typical Shuttle trajectory. The STS source model was developed by analysis of pressure data recorded during STS launches at Kennedy Space Center (KSC).[2,3] This equivalent source satisfies the STS acoustic emissions near the time of peak pressure loading and as observed at an open, flat-earth, 300 m from the LM. The explosion response terms were measured in the "as-built" GSS facilities and contain all V23 site particular information including the effects of reverberations due to topography, large structures, and seismic coupling with the acoustic source. Under the analysis conducted for this report, the structural response term is considered deterministic,

References 1, 2, and 3 will not be listed here. See References, page 57.

while the STS source term carries the statistical variability of the forecasting algorithm.

At the time of the VAFB sounding tests, March 1984, construction at V23 was incomplete although all major structures had been erected. The most significant work yet to be completed was the installation of siding on the Shuttle Assembly Building (SAB). In addition, some welding of steel plates at the west end of the Orbiter Functional Simulator (OFS) room was in progress. Although the incomplete state of V23 will cause some change in the predicted vibro-acoustic environment, it is believed that the unfinished work will not materially degrade the forecasts.

## 2. FINDINGS

### 2.1 Overview

Using the techniques discussed in this and previous reports, Air Force Geophysics Laboratory (AFGL) has been able to produce forecasts of the launch induced vibro-acoustic environments at a number of locations at V23.[1] The sites examined in these studies were selected by the Shuttle Activation Task Force (SATAF) and were confined to the PPR, PCR, and AB. The original experimental plan called for a more comprehensive study including explosive response measurements in the Mobile Service Tower (MST), SAB, Launch Control Center (LCC) and on the Access Tower. However, due to conflicts with the V23 construction schedule, the second, more comprehensive, phase of this study was cancelled by SATAF.

The GSS facilities at V23 do not have specific launch induced motion levels imposed as design specifications. It is apparent, however, that levels of concern can be established against which one can evaluate the severity of the forecast vibro-acoustic environments. Levels of concern have been derived from historic usage, physical implications, or limitations established for equipment intended to be located in the vicinity of specific sites. The definitions of these levels and the derivation of the criteria are given in Section 3.

It must be noted, however, that these values were selected merely as reference levels to highlight unusually severe or unexpected vibro-acoustic environments. AFGL does not represent them to be design specifications. It must be the responsibility of the appropriate offices within SATAF to evaluate the significance and implications of exceeding criteria cited in this report.

## 2.2 Vibration Environment

Motion levels of concern are forecast to be approached or exceeded at four locations in V23. Specifically, these locations are:

(a) The upper Payload Ground Handling Mechanism (PGHM) rail in the PCR, where acceleration criteria were exceeded.

(b) The lower PGHM rail in the PCR, where acceleration criteria were also exceeded.

(c) The gap between the PCR and the PPR, in launch configuration, where pounding could occur.

(d) The OFS room of the AB, where strong vertical accelerations are forecast.

The presented forecasts are expected value predictions and do not reflect conditions resulting from unusual trajectories or acoustic power variations in STS rocket motors. The impact of the ignition pulse has also been largely suppressed in this analysis. A brief summary of the vibration forecasts for each facility follows.

### 2.2.1 PAYLOAD PREPARATION ROOM

Specific criteria were established in the Payload Requirement Document for the vibration environment in the PPR.[4] Motion forecasts at Levels 69, 99, and 119 of Checkout Cell 2 in the PPR do not approach these criteria. At Level 69 the forecasts were made for the cell rail footings and, at all other levels, for the platform to cell rail connection. Peak accelerations at all locations were forecast to be less than 0.07 g. As the peak acceleration forecasts are substantially below the root mean square (rms) acceleration criteria for the PPR, it can virtually be assured that the rms criteria will not be exceeded. Similarly, Power Spectral Density (PSD) levels are at least one order of magnitude below the PSD criteria, 0.01 $g^2$/Hz. Motion forecasts by AFGL are significantly lower than previous finite element (FE) model results.[5] The FE model includes thrust augmentation, which was not considered in this report.

One caveat must be attached to the preceding discussion. The acceleration levels forecast for the PPR assume that pounding does not occur between the PPR and PCR. In the event of pounding, higher, but unpredicted, levels of acceleration can be expected throughout the PPR.

---

4. Martin Marietta Corp. (1980) Payload Requirement Document, VCR-77-081, Rev D.

5. Yang, R.C., and Teegarden, W.T. (1980) Part III, Vibro-Acoustic Study, Payload Preparation Room Summary Report, Martin Marietta Corp., VCR-79-145.

2.2.2 PAYLOAD CHANGEOUT ROOM

Based on a measured minimum separation of the PPR and PCR of no more than 4.0 cm at elevation 276 ft (see Figure 2), a high risk exists that launch generated side-on pressures on the PCR will cause pounding between the PCR and PPR.[1] The PCR exhibits a lightly damped sway when driven by acoustic pressures originating over the LM. Westward sway of the PCR towards the PPR will regularly exceed 2 cm, one half of the pre-launch gap. This was the designated level of concern. Due to the major structural change in the PPR at elevation 165 ft, it is impossible to estimate the eastward displacements of the PPR Transfer Tower from the data available at lower floors. It is significant to note that for one in every 20 to 30 launches the sway of the PCR alone will be sufficient to close the gap completely without requiring any motion of the PPR tower.

A 4 cm at rest gap between the PCR and PPR is probably insufficient to consistently accommodate sway in both structures. If so, these structures will pound during launch. Estimation of the rebound characteristics, resulting damage, and subsequent effects are beyond the scope of this study. It can be assumed that high accelerations throughout the PCR and PPR will be induced by pounding.

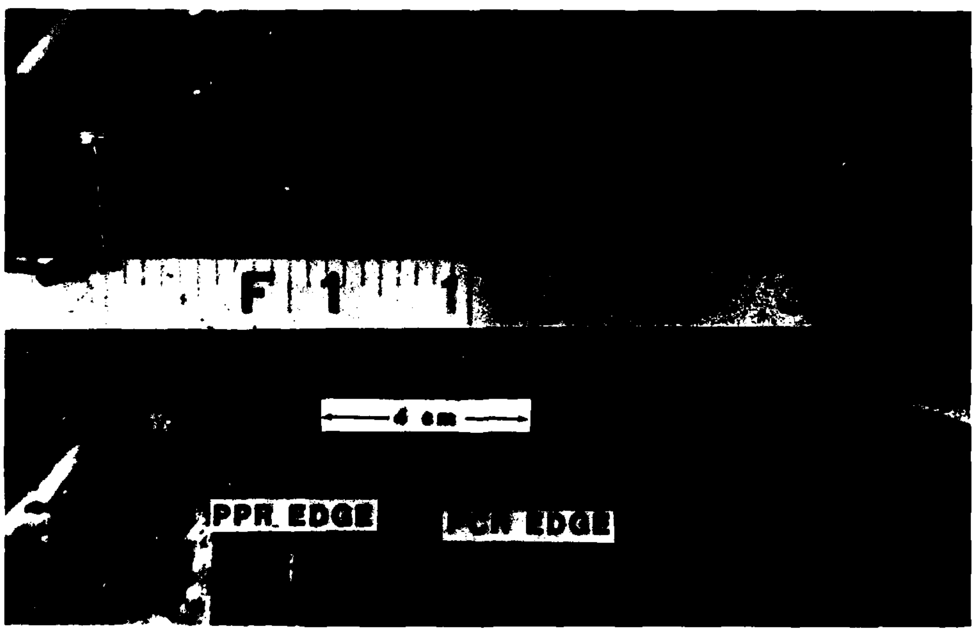


Figure 2. Photograph Showing the Separation of the PPR and PCR at Elevation 276 ft. (Scale in Tenths of Feet)

The Payload Requirements Document[4] specifies that PCR/PGHM rail accelerations will not exceed 0.5 g in any one direction or 0.1 g over the frequency band of 2 to 100 Hz. Peak accelerations forecast for the lower PCR/PGHM rail are in excess of 0.55 g over the narrow frequency band of 0.4 to 30 Hz (Figure 3). Extension of the frequency range can only increase the peak forecast amplitude. All individual components on the PCR/PGHM rail approach or exceed the specified 0.1-g criteria. Further, the general PSD level of concern, 0.01 $g^2$/Hz, is exceeded on the east component of the upper PGHM rail and on the vertical component of the lower PGHM rail (Figures 4 and 5).

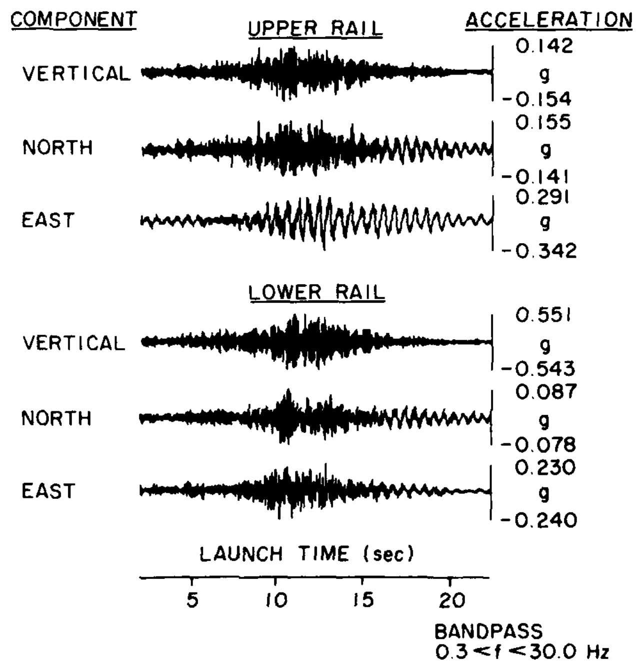


Figure 3. Forecast Acceleration Time Histories for the Upper and Lower PCR/PGHM Rails on the South Side of the PCR

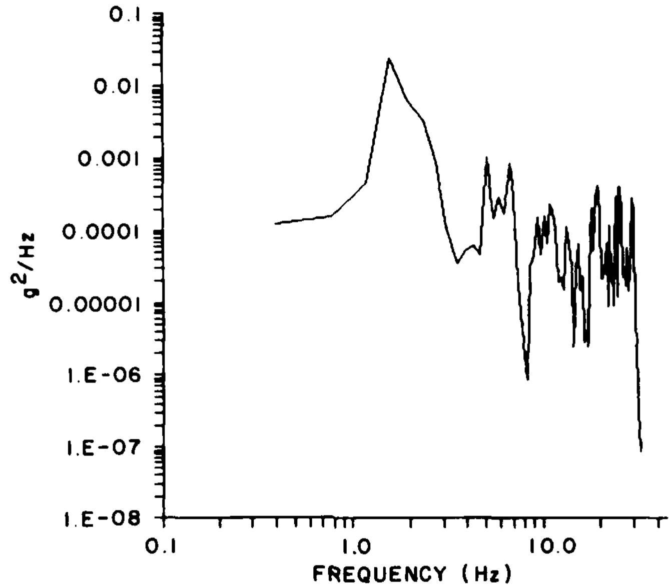


Figure 4. Forecast PSD Plot for the South Upper PCR/PGHM Rail Accelerations in the East-West Direction

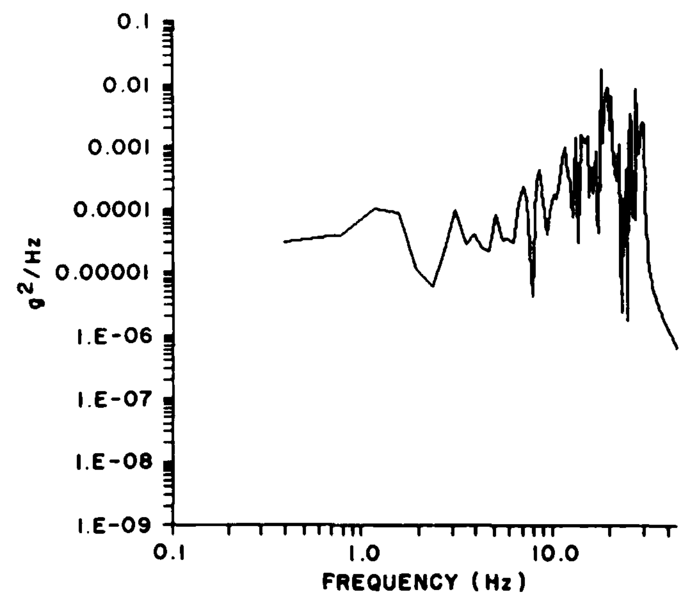


**Figure 5. Forecast PSD Plot for the South Lower PCR/PGHM Rail Accelerations in the Vertical Direction**

2.2.3 ORBITER FUNCTIONAL SIMULATOR ROOM

Floor accelerations forecast in the OFS room of the AB indicate peak vertical accelerations at this location will approach, and might easily exceed 1 g.[1] Horizontal peak accelerations are significantly lower, typically about 0.15 g. Actual forecast amplitudes for the vertical peak accelerations exceed 0.7 g (Figure 6). The forecasts are based on a source located over the LM. As the Shuttle climbs and rotates to the south, roof loading will increase on the AB. As a consequence, accelerations in this building can also be anticipated to exceed the forecasts. The accelerations exceed both generic and specific levels of concern. First, vertical accelerations approaching 1 g raise questions about the structural integrity of any building. Second, vibration tests on equipment similar to that intended for the OFS room were run only to 1.0 g. The capability of this equipment to operate after being subjected to accelerations above this level is open to question.

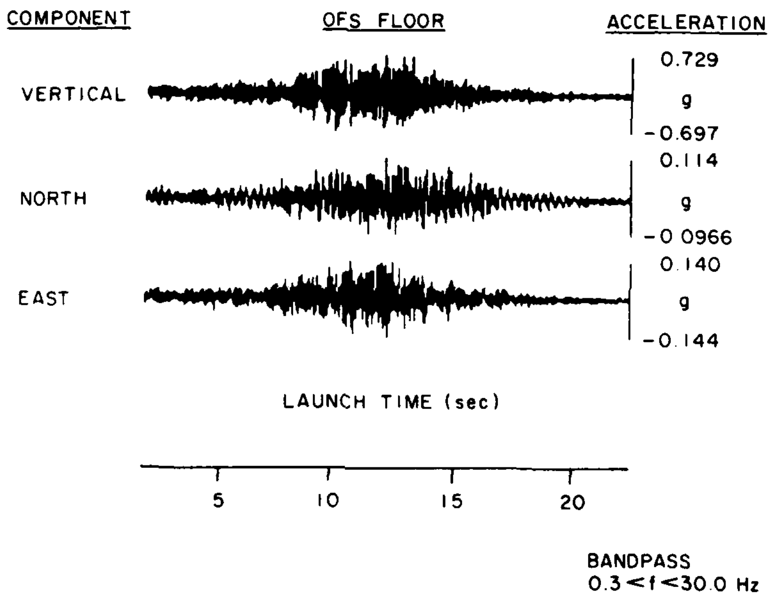


Figure 6. Forecast Acceleration Time Histories for the OFS Room Floor

## 2.3 Acoustic Environment

During the AFGL Phase I Sounding Program at VAFB, pressure transducers were located on the east face of the PPR, the AB roof, and at 49 m west of the V23 LM. Analysis of the explosion responses from these locations shows strong, persistent reverberations.[1] These reverberations will significantly alter the

magnitude, phase, and spectral characteristics of acoustics emitted from any source above the LM.

Pressure spectral levels forecast for the east face of the PPR and roof of the AB are as much as 14 dB greater than those observed at an equivalent distance at an open, flat-earth, launch facility such as KSC (Figure 7). For the same locations, overall sound power levels (OASPLs) on exposed walls are forecast to be more than double flat-earth values.

The method used to forecast acoustic loads has not been tested in the near-field. Therefore, no forecasts were made for the site at 49 m from the LM. However, analysis of the explosion data taken at this distance also shows a marked alteration of the flat-earth wavelet.[6] These data indicate that pressures found at KSC close-in to the LM cannot be directly applied to V23 due to site peculiar multipathing at V23.

The pronounced reverberations observed at V23 raise questions as to the usefulness and credibility of OASPL contour maps such as those published in the Launch Induced Environment Data Book.[7]

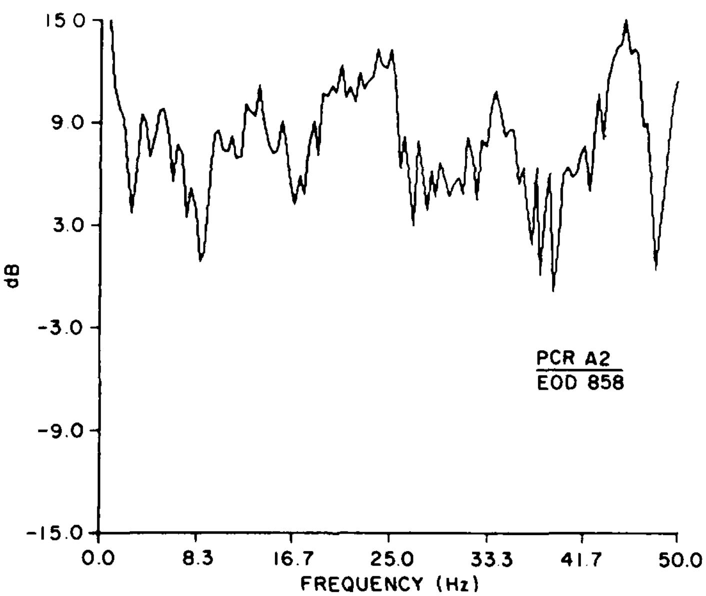


Figure 7. Spectral Ratio for the Acoustic Loads at the East Face of the PPR With a Flat-Earth Site at the Same Distance

6. Crowley, F.A. (1985) Personal Communication, Boston College.

7. Allen, T. (1982) Launch Induced Environment Data Book, Martin Marietta Corp., VCR-82-293.

### 2.4 Seismic Hazards

The AFGL Sounding Program was directed to evaluation of launch induced environments in GSS facilities. Through this effort, however, certain other questions have been raised that are not launch related, but should be of concern to SATAF. Specifically, these questions concern the potential for pounding between various structures at V23 due to earthquake ground motions.

Vandenberg AFB is located in one of the most seismically active regions of the continental United States.[8] Historic activity has produced Modified Mercalli intensities as high as IX in the L. npoc area. Such an intensity implies considerable damage even to specifically designed structures, including partial collapse. In addition, numerous faults near the facility have been identified as having Quaternary displacements, taken to be an indication of continuing potential for seismic activity.

When subjected to earthquake ground motions, each structure at V23 will exhibit some level of sway displacement, horizontal motion increasing with the height of the building. If insufficient clearance is allowed, earthquake-induced sway will result in pounding between buildings. The potential exists for damage to equipment due to high accelerations caused by the pounding or even structural damage.

The building responses obtained in the Sounding Program are for acoustic loading and cannot be used to evaluate the seismic excitation of the structures at V23. However, these data do suggest several situations where pounding could occur during moderate earthquakes. First, it can be anticipated that pounding could occur between the AB and PPR. It is noted that the maximum design gap between these buildings (15.3 cm)[9] corresponds to a ground displacement having a 10 percent probability of occurrence in any 20-year period.[8] This is a lower limit on the probability as the ground displacement will be amplified by the response characteristics of the PPR and AB. Similarly, earthquake-induced sway of the PPR and PCR, in launch configuration, could cause pounding. In this case, the 20-year period probability of ground displacement exceeding the gap between the buildings is greater than 90 percent. To evaluate the likelihood of pounding, this probability must also be modified for the effects of structural responses and for the fraction of time the two structures are in launch configuration. Finally, it is anticipated that some risk of pounding during earthquakes will also incur due to the close pro imity of structures when at the LM, MST, SAB, PCR, and Shuttle.

8. Battis, J.C. (1979) Seismic Hazards Estimation Study for Vandenberg AFB, AFGL-TR-79-0277, AD A082458.

9. Johnson, D.P. (1985) Comparison of Launch Induced Vibro-Acoustics: Analysis and AFGL Sounding Test, Martin Marietta Corp., Draft Report.

Individual structures at V23 have been designed to seismic zone 4 criteria.[9] However, it is not readily apparent that the seismic hazards of the complex, as an integrated system, have been fully evaluated. With the possible exception of the AB-PPR interface,[9] AFGL has not seen any indication that this subject has been considered in the design of V23. This does not necessarily imply that it has not been considered. The discussion given above is meant only to highlight a potential problem suggested by the Sounding Program results. It is the responsibility of the appropriate offices within SATAF to evaluate the significance of this problem on STS operations.

## 3. LAUNCH ENVIRONMENT CHARACTERIZATION

### 3.1 Overview

The vibro-acoustic environment can be characterized using many different methods of specification. Further, the full implications of any specification are subject to the computational basis used in evaluating the specific value. In this report an attempt has been made to adhere to a set of rigid definitions for specification nomenclature to insure a clear understanding of the terms used in this report and the relation to "like" values reported elsewhere. The definition of each specification is given in the following sections. Where applicable, specific computational parameters associated with these definitions are also stated.

Characterization of the vibro-acoustic environment is of little value unless the significance of the forecast levels can also be judged. For the sites examined in this report there do not appear to be stated launch induced vibro-acoustic specifications against which the forecasted motions can be compared.[10] Based on several lines of argument, however, it is possible to establish "levels of concern" for evaluating the forecasts. In the following sections, the levels of concern used in this report for each of the facilities are defined and justifications for their adoption are provided.

### 3.2 Definitions

#### 3.2.1 VIBRATION SPECIFICATIONS

Vibration forecasts for this study were made over the frequency band of 0.4 to 30 Hz. This bandwidth can be expected to envelop the dominant frequencies of structural response for the GSS facilities. In reality, higher and lower frequencies will contribute to the vibrations observed within each structure and can be

10. (1983) Station Set Specification for VAFB V23 Launch Pad 1 Station Set, Specification No. SSS-2300B, Modification No. 50.

expected to modify the predicted motions. However, these modifications would not be expected to be substantial.

To characterize the motion environments at V23 the following measures were used:

(a) Peak Motion - The maximum, single component amplitude of motion away from the long term rest value.

(b) rms Value - The root mean square amplitude of a single component of motion away from the long term rest value over a duration T starting at time $t_o$. All rms values given here are for a duration of 1.5 sec starting 0.75 sec prior to the occurrence of the peak motion on a given trace.

(c) PSD Level (Power Spectral Density Level) - The periodogram average for one component of motion using a sample duration of T starting at time $t_o$. For PSD level evaluations, the duration is fixed at 2.56 sec starting 1.28 sec prior to the occurrence of the peak motion amplitude on a given component.

(d) Pseudo-Velocity Response Spectra - The plot, with respect to natural frequency, f, of the peak motion amplitude for a 1-degree of freedom (DOF) system having a natural frequency of f and driven by a specified single component velocity time history.

Dampings of 2 and 5 percent were used in all response spectra plots. These dampings are typical lower and upper limits for most building modes.

3.2.2 PRESSURE SPECIFICATIONS

The measures of acoustic pressure used in this report are:

(a) Peak Pressure - The largest pressure deviation from the ambient observed for any single instrument.

(b) OASPL - The integral of the standard form Shuttle spectrum obtained by fitting the spectrum over the band 0.4 to 50 Hz to forecast spectra.

The standard form Shuttle spectrum is given in Appendix B.

### 3.3 Levels of Concern

To highlight the relative severity of the vibro-acoustic environments forecast at each location, the motions were compared with certain levels of concern. After review of the relevant sections of the V23 Station Set Specification[10] it does not appear that GSS facilities have definitive launch environment specifications. However, a review of various documents dealing with the launch induced vibro-acoustic environment suggests certain motion and pressure values that can be cited as levels of concern. In addition, either historical usage or simple physical implications are also used to justify these levels of concern.

It should be noted that the use of levels of concern is merely intended to highlight relatively severe launch environment conditions. The significance of

approaching or exceeding these values is a subject that must be determined by the responsible offices of SATAF.

Levels of concern have been divided into two categories, general and site specific. The general criteria have been established on the basis of historical usage. Site-specific levels are typically derived from the literature on V23 or based on clear physical implications. As a hierarchy, exceedance of a site-specific criterion should be deemed more significant than exceedance of a general criterion.

### 3.3.1 GENERAL LEVELS OF CONCERN

The first general level of concern is:

(a) Acceleration PSD - An acceleration PSD of 0.01 $g^2$/Hz at any frequency. This has historically been used as a generic level of concern since AFGL has been associated with this subject.[11, 12] In addition, it has been used by others in vibration analysis of GSS facilities to which it does not strictly apply.[13]

(b) rms Acceleration - An rms acceleration of 0.7 g in the frequency band below 50 Hz. This statement is an approximate time domain equivalent to the acceleration PSD level of concern.

(c) Peak Vertical Acceleration - A peak vertical acceleration of 0.7 g. Any vertical acceleration approaching 1 g must bring into question the structural integrity of the impacted building.[13]

(d) Pseudo-Velocity Response - A spectral peak of 254 cm/sec at any frequency. This level is taken to be a pseudo-velocity response amplitude equivalent to the general PSD level of concern.[14]

(e) OASPL - Exceedence of OASPLs observed at KSC for Shuttle launches. OASPLs forecast for KSC on the basis of extrapolation of Saturn launch data have been used to support design and analysis of V23 facilities.[7] The published Saturn data values are not equivalent to AFGL forecast OASPL values. This is due to differences in averaging time used by National Aeronautics and Space Administration (NASA) and AFGL. Further, the KSC values are for 97.7 percent non-exceedance level while AFGL estimates are expected (50 percent) or mean values.[15]

---

11. Crowley, F.A. (1985) Personal Communication, Boston College.
12. Smith, J. (1985) Personal Communication, Aerospace Corp.
13. Zagzebski, K.P. (1978) Launch Induced Vibro Acoustics Analysis, Launch Control Center, Ralph M. Parsons Co., TOR No. 114.
14. Wheeler, R.H., and Teegarden, W.T. (1982) Launch Induced Vibration Assessment, Final Report, Martin Marietta Corp., VCR-82-337.
15. NASA (1976) Environment and Test Specification Levels: Ground Support Equipment for Space Shuttle System Launch Complex 39, Acoustic and Vibration, Vol. I, GP-1059, Rev A.

### 3.3.2 SITE-SPECIFIC CRITERIA

#### 3.3.2.1 Payload Preparation Room

The Payload Requirements Document[4] specifies the following level of concern for the PPR:

(a) Acceleration PSD - An acceleration PSD of 0.01 $g^2/Hz$ over the frequency band 20 to 2000 Hz.

(b) rms Acceleration - An rms acceleration of 4.4 g over the frequency band of 20 to 2000 Hz. This criterion is equivalent to 0.5 g over the band of 0.4 to 30 Hz based on an adjustment for the different bandwidth used for forecasting.[5]

#### 3.3.2.2 Payload Changeout Room

The Payload Requirements Document specifies "equivalent steady-state acceleration" criteria for "induced loads" on the PCR/PGHM rail.[4] For the purposes of this study these steady-state values are assumed to be equivalent to peak acceleration values. Then, the two peak acceleration levels of concern are:

(a) A peak acceleration of 0.5 g in any one direction over all frequencies; or

(b) A peak acceleration of 0.1 g in any one direction in the frequency band of 2 to 100 Hz.

Separation between the PCR and PPR in launch configuration has been measured to be no more than 4.0 cm at elevation 276 ft (Figure 2). This is in contrast to the construction drawings that show a separation of 10 cm.[9] To prevent pounding between these structures, the combined westward displacement of the PCR and eastward displacement of the PPR must be less than this amount. Due to the curtailment of the Sounding Program, eastward PPR displacement at this level can not be forecast. Therefore, lacking better solutions, a westward displacement criterion for the PCR was established as one-half of the pre-launch gap. This level of concern is:

(a) Peak Sway Displacement - A peak westward displacement of 2 cm.

#### 3.3.2.3 Orbiter Functional Simulator Room

Equipment intended to be placed in the OFS room has been tested to 1.0 g peak acceleration.[12] Any forecast acceleration that approaches or exceeds the test limits should be of concern. Thus, a level of concern for the OFS room is established to be:

(a) Peak Acceleration - A peak acceleration approaching 1.0 g.

## 4. FORECASTING PROCEDURE

### 4.1 Overview

The response, u(t), of a time invariant, linear system to a specified driving function, d(t), can be expressed as the convolution of the system impulse response wavelet, h(t), with the driving function[16]

$$u(t) = h(t) * d(t) \quad . \tag{1}$$

In this form, the impulse response wavelet is a unique characterization of the system. Making a reasonable assumption that structures not close to failure behave as time invariant, linear systems, it can be seen that Eq. (1) provides a basis for forecasting launch induced vibration environments at V23. By measuring the vibration response at some location, $u^E(t)$, caused by a known driving function, $d^E(t)$, such as an explosion, one can recover the impulse response wavelet, h(t), for that location. As h(t) is unique to the structure and independent of the driving function, a forecast of launch motions, $u^{STS}(t)$, can be made by convolving the derived impulse response wavelet with an appropriate model for the STS launch acoustics, $d^{STS}(t)$.

While providing a simple statement of the forecasting technique used in this study, this description evades both the details and assumptions required for practical implementation. In the following paragraphs, a derivation of the actual methodology is presented. While not all of the nuances of the problem are discussed, the significant limitations of the forecasting process are presented.

### 4.2 The Pressure Functions

Before deriving the actual forecasting algorithm, it is useful to consider the forms that will be used to represent the explosive and Shuttle generated acoustic signal. In particular, the Shuttle pressure representation will influence the final form of the forecasting algorithm. Throughout these discussions, consideration will be limited to that domain of acoustic propagation where attenuation is inversely proportional to range, r.

It should be apparent from the nature of the source that the acoustic output of a small, elevated charge, observed at distances many times larger than the source dimensions, can be represented as emanating from a point (monopole) source. Further, the acoustic emissions propagate away from the source under

16. Jenkins, G.M., and Watts, D.G. (1969) Spectral Analysis and Its Applications, Holden-Day, San Francisco.

the laws of spherical acoustics. For a flat, perfectly reflecting earth away from any obstructions, the explosive pressures at a point can be modeled as

$$p^E(t, r) = (r_o/r)\, g^E(t - [\{r - r_o\}/c],\, r_o) \quad , \tag{2}$$

where r is the source to observer range, $r_o$ is a reference range, $g^E(t, r_o)$ is the pressure wavelet modeled at $r_o$, and c is the speed of sound in air. The term $[\{r - r_o\}/c]$ defines the propagation time shift of the waveform between the reference and observation points. Similarly, the spectral form of the explosive pressure wavelet is given by

$$P^E(f, r) = (r_o/r)\, G^E(f, r_o) \quad , \tag{3}$$

where f is frequency and $G^E(f, r_o)$ defines the amplitude and spectral shape of the acoustic transient at the reference distance. (Throughout the remainder of this section, a capital letter is used to represent the spectral equivalent of a time series specified by the respective lower case letter.) The specific nature of $G^E(f, r_o)$ is of little consequence to the theoretical development that follows. However, the actual form of $g^E(t, r_o)$, and thus of $G^E(f, r_o)$, was obtained empirically and is given in Appendix B.

It has been shown in previous studies that the acoustics of a rocket exhaust can also be adequately described at a flat earth site as an axial symmetric source that travels with the rocket but somewhat below it in the exhaust plume.[2, 3, 17] For an STS launch, significant acoustic loads are observed on the ground for approximately 30 sec following main engine ignition. Once clear of the ground, the spectral shape of the acoustic signal remains relatively constant and is well described by a theoretical form proposed by Powell for undeflected, plume generated acoustics (see Appendix B).[18] The most significant divergence from this theoretical shape occurs early in the launch sequence when the exhaust plume interacts with the ground and during Solid Rocket Booster (SRB) ignition. At these times pressures of concern are low compared with peak values and the change in spectral shape is not expected to greatly affect the forecast results.

While the spectral shape remains reasonably constant throughout the launch, the level of the spectrum, as observed at a fixed point on the ground, changes throughout the launch. In part, this variation occurs as a result of the increasing

---

17. Crowley, F.A., Hartnett, E.B., and Ossing, H.A. (1980) The Seismo-Acoustic Disturbance Produced by a Titan III-D With Application to the Space Transportation System Launch Environment at Vandenberg AFB, AFGL-TR-80-0358, AD A100209.

18. Powell, A. (1964) Theory of vortex sound, J. Acoust. Soc. Am. 36:177-195.

distance to the source. More significantly, the acoustic radiation pattern of the rocket source is not spherical but exhibits distinct directivity.[17] For a fixed observer, however, the source directivity and range effect (for repeated launches over the same trajectory) can be equated to a time dependent variation in the source strength. In other words, a source, stationary in space, can be defined that, for a fixed observer, represents the moving source by varying the amplitude of the source emissions.

The STS launch pressures, at a point on a perfectly reflecting earth, can be modeled as an independent, identically distributed normal process modified to give the correct spectral shape and time dependence. Mathematically, this model has the form

$$p^{STS}(t, r) = g^{STS}(t, r) * [n(t) \cdot e(t, r)] \quad , \tag{4}$$

where $p^{STS}(t, r)$ is the acoustic wavelet at the point, $r$ is the source range, $g^{STS}(t, r)$ is a shaping wavelet that produces the correct amplitude and spectral shape at the time of peak pressure loading, $n(t)$ is a realization of a zero mean, unit variance, normal process, and $e(t, r)$ is an envelope function that controls the apparent source strength. Again, the exact nature of the individual terms have no consequence for the derivation that follows.

At this time, the pressures due to a rocket source have been defined at only one point. What is ultimately required, however, is the distribution of pressures on a surface.[15] For the explosive source, the required distributions can be obtained by extrapolation from the pressure at the given point by the laws of spherical acoustics. This is a consequence of the point source nature of the explosion. For areas comparable to the exposed surface areas of structures at V23, this extrapolation process has also been shown to be valid for a rocket source, including STS launch pressures.[2, 3, 17] This implies that the range dependent elements of $p^{STS}(t, r)$, that is, $g^{STS}(t, r)$ and $e(t, r)$, vary only slowly with range. Over relatively large areas, then, the STS pressures can be viewed as having an equivalent point source representation. In this case, however, the parameters of the point source model must be adjusted for gross changes in the range of interest. Then, the STS acoustic pressures can also be specified in a form similar to Eq. (2) as

$$p^{STS}(t, r) = (r_o/r)\, g^{STS}(t - [\{r - r_o\}/c], r_o) * [n(t) \cdot e(t, r_o)] \quad , \tag{5}$$

with the frequency domain representation given by

$$P^{STS}(f, r) = (r_o/r)\, G^{STS}(f, r_o) \cdot [N(f) * E(f, r_o)] \quad . \tag{6}$$

The definition of $G^{STS}(f, r_o)$ is given in Appendix B.

It should be noted that potentially significant information is lost in using this representation for the Shuttle acoustic pressures. Consider two point sources, A and B, and two observation points, C and D, as shown in Figure 8. Using the stationary point model for the STS acoustics, the phase relationship between the signals arriving at points C and D will always remain the same. Any pressure pulse emitted by source A will arrive at C and D simultaneously as both points are an equal distance from the source. If the source was to move to B, the distance between the source and the two observation points would no longer be the same and a pressure pulse from source B reaches the observation points at times separated by a travel time difference of $\Delta t$. Thus, in the case of a moving source, the relative distribution of pressures on a surface will vary with time while for the stationary source the relative distribution will be fixed. As it is the spatial and temporal variation of the pressures that determine the induced motions of the structure, the stationary source cannot fully represent the effects of a moving source. It remains to be seen to what degree this simplification will degrade the forecast results.

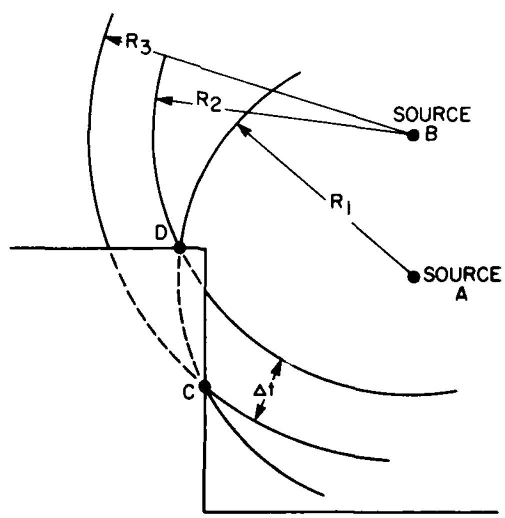


**Figure 8. An Illustration of the Effect of Source Motion on the Phasing of Loads on a Structure**

### 4.3 The Forecasting Algorithm

In the simplified statement of the forecasting algorithm given in Eq. (1), the problem was stated in terms only of the variable time, t. As the driving load on a structure can be applied at any point, or set of points, on the surface of the structure, Eq. (1) must be expanded to include this spatial dependence. Initially, only acoustic loads on the structure of interest are considered. As will be shown later, this development can be readily expanded to include induced seismic loads through a redefinition of the boundaries of the linear system.

Considering a structure to be a time invariant, linear system, Eq. (1) can be re-interpreted as defining the relationship between the $k^{th}$ component of motion, $u_k$, at some location on the structure defined by a coordinate vector $\underline{x}$, and the causative loading function, d, applied at a point defined by the vector $\underline{y}$. Then, a *unique impulse response* wavelet, $h_k(t, \underline{x}, \underline{y})$, exists connecting the motions induced by the driving function such that

$$u_k(t, \underline{x}, \underline{y}) = h_k(t, \underline{x}, \underline{y}) * d(t, \underline{y}) \cdot \Delta S \quad , \tag{7}$$

where $\Delta S$ is the area over which the load is applied. Note that $u_k$ is dependent on both the location of the observation point and the point of load application. It is also noted that, as only acoustic loads are considered, the applied load is, by definition, normal to the surface of the structure and the usual component index is not required for the loading function. For the problem under consideration, an acoustic source external to the structure, the location of the driving force, given by $\underline{y}$, can be restricted to the exterior surface of the building.

Introducing superscript notations to distinguish source type, the equation for the explosion becomes

$$u_k^E(t, \underline{x}, \underline{y}) = h_k(t, \underline{x}, \underline{y}) * d^E(t, \underline{y}) \cdot \Delta S \tag{8}$$

and for an STS source by

$$u_k^{STS}(t, \underline{x}, \underline{y}) = h_k(t, \underline{x}, \underline{y}) * d^{STS}(t, \underline{y}) \cdot \Delta S \quad , \tag{9}$$

where $h_k(t, \underline{x}, \underline{y})$ is identical in both cases. The equivalent frequency domain representations are

$$U_k^E(f, \underline{x}, \underline{y}) = H_k(f, \underline{x}, \underline{y}) \cdot D^E(f, \underline{y}) \cdot \Delta S \tag{10}$$

for the explosion and

$$U_k^{STS}(f, \underline{x}, \underline{y}) = H_k(f, \underline{x}, \underline{y}) \cdot D^{STS}(f, \underline{y}) \cdot \Delta S \tag{11}$$

for the Shuttle launch. It follows that the impulse response spectrum, $H_k(f, \underline{x}, \underline{y})$, can be evaluated from Eq. (10) as the spectral ratio of the explosion motions to the explosive driving function. Substituting that quantity into Eq. (11) yields

$$U_k^{STS}(f, \underline{x}, \underline{y}) = U_k^E(f, \underline{x}, \underline{y}) \cdot [D^{STS}(f, \underline{y})/D^E(f, \underline{y})] \cdot \Delta S \tag{12}$$

and relates the observed explosion motions to the STS induced motions.

Consider the spectral ratio of the driving functions, $[D^{STS}/D^E]$. For a common atmosphere, spherical acoustic propagation is, itself, a linear time-invariant system. If the explosion and STS pressures can be represented as propagating from point sources, as was shown in the previous section, then extrapolation of the pressures from any reference location to the point of load application can be represented in the form of Eq. (1). Then, the driving functions for each source type can be represented by

$$D(f, \underline{y}, \underline{z}) = H^P(f, \underline{y}, \underline{z}) \cdot P(f, \underline{z}) \quad , \tag{13}$$

where $H^P(f, \underline{y}, \underline{z})$ is the propagation response spectrum and $P(f, \underline{z})$ is the spectral representation of the pressure wavelet at a location specified by the coordinate vector $\underline{z}$. As before, $H^P(f, \underline{y}, \underline{z})$ is independent of the type of acoustic source driving the system. The spectral ratio of the driving functions, for a common source location, is then seen to be given by

$$D^{STS}(f, \underline{y}, \underline{z})/D^E(f, \underline{y}, \underline{z}) = P^{STS}(f, \underline{z})/P^E(f, \underline{z}) \tag{14}$$

and is dependent solely on the source location and independent of the point of load application.

Substituting Eq. (14) into Eq. (12) provides the frequency domain representation of a fundamental relationship between the STS and explosion induced motions, or

$$U_k^{STS}(f, \underline{x}, \underline{y}, \underline{z}) = U_k^E(f, \underline{x}, \underline{y}, \underline{z}) \cdot [P^{STS}(f, \underline{z})/P^E(f, \underline{z})] \cdot \Delta S \tag{15}$$

and, with conversion into the time domain, one obtains

$$u_k^{STS}(t, \underline{x}, \underline{y}, \underline{z}) = u_k^E(t, \underline{x}, \underline{y}, \underline{z}) * v(t, \underline{z}) \cdot \Delta S \quad , \tag{16}$$

where $v(t, \underline{z})$ is some wavelet, referred to as the driving wavelet, defined by the inverse transform of the spectral ratio of pressure functions for the STS launch and the explosion.

So far, this derivation has treated the motions at $\underline{x}$ due to loads applied at a single point on the surface of the structure, specified by the vector $\underline{y}$. In fact, the loads are distributed over the entire surface of the structure and the motions for an STS source located at $\underline{z}$, $u_k^{STS}(t, \underline{x}, \underline{z})$ will be given by the integral of $u_k^{STS}(t, \underline{x}, \underline{y}, \underline{z})$ over the surface of the structure

$$u_k^{STS}(t, \underline{x}, \underline{z}) = \int u_k^{STS}(t, \underline{x}, \underline{y}, \underline{z})\, dS \tag{17}$$

or from Eq. (16)

$$u_k^{STS}(t, \underline{x}, \underline{z}) = \int u_k^{E}(t, \underline{x}, \underline{y}, \underline{z}) * v(t, \underline{z})\, dS \quad . \tag{18}$$

As $v(t, \underline{z})$ is independent of the load application point, the integral reduces to

$$u_k^{STS}(t, \underline{x}, \underline{z}) = u_k^{E}(t, \underline{x}, \underline{z}) * v(t, \underline{z}) \quad , \tag{19}$$

where $u_k^{E}(t, \underline{x}, \underline{z})$ is the total motion produced by an explosion at $\underline{z}$ and observed at $\underline{x}$, the quantity observed during the AFGL Sounding Program.

Under this construction, the time invariant, linear system used in the forecast scheme has been expanded from just the structure to include the entire propagation process between the point source and the location at which the motions were observed. As stated earlier, this derivation was made assuming only acoustic loads. As with acoustic propagation, seismic propagation can be treated as a time invariant, linear system. By redefining the surface of the structure to include the surface of the ground, acoustic coupled seismic loading will also be covered by this forecasting algorithm. In a strict sense, only the seismic loads generated by coupling in the far-field will be accurately forecast by this algorithm. Seismic loads induced near the LM, when the Shuttle is not far above the ground, would not be expected to be accurately forecast by this method. This results from the inadequacy of the Shuttle source model to represent the pressure distributions on the ground close-in to the LM early in lift-off.

### 4.4 The Driving Wavelet

What remains, then, is to define the driving wavelet, $v(t, \underline{z})$ used in the forecasting algorithm given by Eq. (19). From Eq. (14), the spectrum of the driving wavelet, $V(f, \underline{z})$, is defined by the spectral ratio of the STS pressure model to the explosive model. As defined, the driving wavelet is a function of source location, $\underline{z}$. In developing the STS pressure model a stationary source was assumed. For the explosion source, a fixed source location is axiomatic. As a result of these assumptions and for collocated sources, the dependence on $\underline{z}$ can be converted to a dependence on range, r. From Eqs. (3) and (6)

$$V(f, r) = [G^{STS}(f, r_o)/G^{E}(f, r_o)] \cdot [N(f) * E(f, r_o)] \tag{20}$$

with the restriction that $G^{STS}(f, r_o)$ and $G^{E}(f, r_o)$ are evaluated at the same reference range, $r_o$. Under these conditions, that is, fixed sources and pressure functions evaluated at the same reference range and boundary conditions, $V(f, r)$ is, in fact, independent of r, the range to the point of loading, but dependent on the reference range and can be reduced to $V(f, r_o)$. (As stated in the development of the STS pressure function, this representation can only be used over limited ranges of r and dependence on $r_o$, the reference range, is significant.) The spectral ratio of the pressure shaping wavelets, the G terms, is defined as the shaping spectrum, $W(f, r_o)$.

In the time domain, $v(t, r_o)$ is given by

$$v(t, r_o) = w(t, r_o) * [n(t) \cdot e(t, r_o)] \quad , \tag{21}$$

where $w(t, r_o)$ is the shaping wavelet and is defined solely by the inverse transform of the spectral ratio of the source models, $W(f, r_o)$. The theoretical form of $G^{STS}(f, r_o)$ used in this analysis provides no phase information and it is necessary to assume the phasing of $W(f, r_o)$ to perform the inverse transformation. This requirement is met by specifying that the operator, $w(t, r_o)$, be realizable and of minimum phase.[19]

### 4.5 Conclusions

At this point all terms and relationships required for the forecast procedure have been defined and the final form of the algorithm can be derived. The final formulation is obtained by combining Eqs. (19) and (21) and noting the loss of dependency on the source location, $\underline{z}$, as a result of the assumption of a fixed

---

19. Robinson, E. A. (1967) Statistical Communication and Detection, Griffin, London.

source for both the Shuttle and explosion acoustics. This final construction is given by

$$u_k^{STS}(t, \underline{x}) = u_k^E(t, \underline{x}) * w(t, r_o) * [n(t) \cdot e(t, r_o)] \tag{22}$$

and is the form used to evaluate the STS launch induced motion environments presented in this report.

In deriving this forecast method, the most significant single assumption was that of the stationary source for the STS acoustics. As pointed out in Section 4.2, this assumption can be expected to degrade the forecasts as it is equivalent to stating that the relative distribution of pressure loads on the structure of interest do not change as the Shuttle moves along the launch trajectory. While this assumption is distinctly not true, it is imposed by the impracticality of detonating charges along the initial 30 sec of trajectory to establish the proper phasing of loads during the lift-off sequence.

## 5. THE PAYLOAD PREPARATION ROOM

The PPR is the main VAFB facility for the preparation and testing of payloads prior to their transfer to the Shuttle. It is located approximately 250 m west of the LM. During a launch it can be expected that this structure will house payloads and support equipment for future launches. A plan view of the structure is given in Figure 9 and a cross-sectional view in Figure 10. The locations of each three-component seismometer installation in this study are also shown in Figures 9 and 10. The major elements of this structure are an open transfer aisle along the north wall, the three checkout cells on the south wall, and the Transfer Tower located on the northeast corner. The main structure is of concrete construction, while the Transfer Tower, starting at elevation 165 ft, is a steel frame superstructure through which the payloads pass from the PPR into the PCR.

Each checkout cell consists of a 15.5 by 11.3-m room enclosed by 0.4- and 0.6-m concrete walls in the east-west and north-south directions, respectively. The north wall is broken by the access doors to the transfer aisle. The floor slab under the cells varies in thickness from 0.15 to 0.4 m and access platforms are located up the cell at 3-m intervals. The access platforms are 0.15-m thick concrete. Each platform has a 7.3 by 11.3-m opening in which the payload is positioned for checkout. On the east and west sides of these openings, rails extended the full height of the cell and serve as mounting supports for the payloads while they are in the cells. These rails are coupled to each platform by steel brackets and it is on these brackets that the seismometers were positioned during the

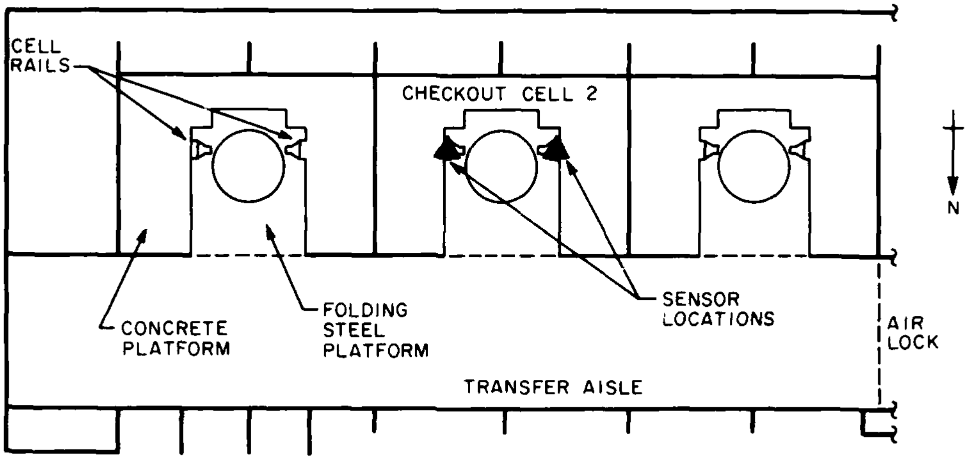


Figure 9. Plan View of the PPR Showing Sensor Locations

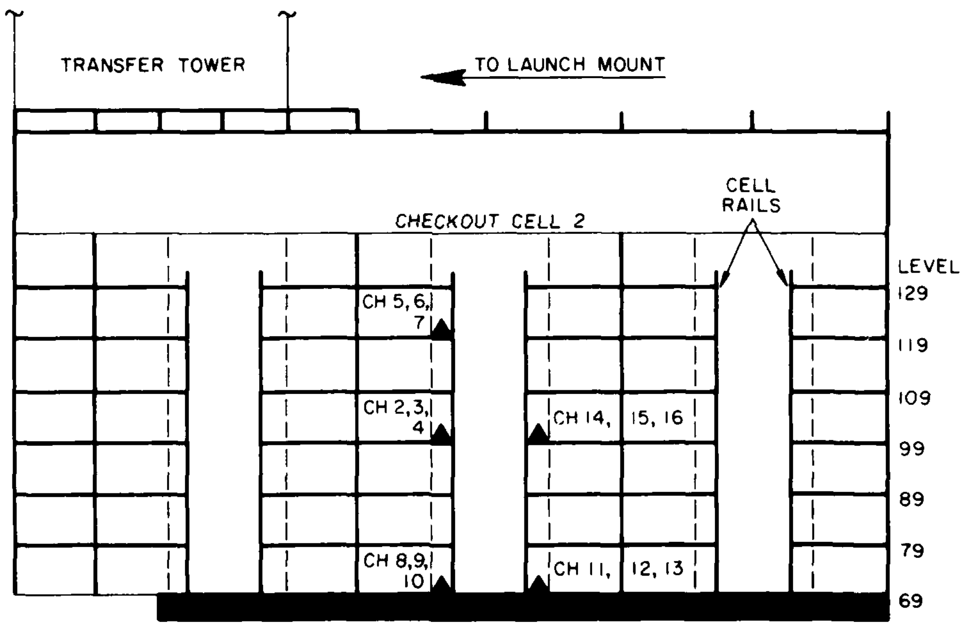


Figure 10. Cross-Sectional View of the PPR Showing Sensor Locations

Sounding Program. At Level 69, the seismometers were placed on the concrete footings of these rails.

## 6. PAYLOAD PREPARATION ROOM FORECASTS

### 6.1 The Shaping Wavelet

The first step in forecasting the STS launch induced motions is to evaluate the shaping wavelet, $w(t, r_o)$, used in Eq. (22). This function is defined from the spectral ratio of the STS acoustic source, at the time of maximum loading, to a 2.3-kg explosive source at a common reference distance. The power spectra of each source, at a reference distance of 300 m, is shown in Figure 11. The appropriate spectral amplitudes and center frequency used to define the STS source had been determined from prior analysis of the acoustic pressures produced by STS Mission 41B.[3] For the frequency band of 0.4 to 30 Hz, the amplitude ratio of these two spectra, the shaping spectrum $W(f, r_o)$, is shown in Figure 12a. The equivalent time domain shaping wavelet, $w(t, r_o)$, obtained by inverse transformation of the shaping spectrum under the minimum phase condition is shown in Figure 12b.

### 6.2 The Envelope Function

The envelope function, $e(t, r_o)$, was computed from the bandpass envelope of the pressure emissions recorded at 300 m from Pad 39A at KSC during the lift-off of STS Mission 41B.[3] This envelope function, shown in Figure 13(a), was generated using a low pass filter with a corner frequency of 30 Hz, essentially matching the bandwidth of the shaping wavelet given above. Figure 13 also shows other envelope functions evaluated using lower corner frequencies. It is significant that as lower cut-off frequencies are used the persistence of the envelope increases and the SRB ignition pulse becomes more pronounced. This implies that the broadband envelope, used in the following analysis, will somewhat underdrive the low frequency modes of the PPR relative to an actual STS launch. The effect should be rather small as the relaxation time of the PPR is less than the separation time of SRB ignition and peak OASPL.

### 6.3 STS Launch Forecasts

Using distinct normal process realizations, $n(t)$, driving wavelets, $v(t)$, for six simulated STS launches were generated. These wavelets were convolved with the observed explosion responses, $u_k^E(t, \underline{x})$, to provide a set of simulated STS launch motion time series. This process was repeated for each of the three shot elevations. In particular, the explosion responses used were from shots A2, B2,

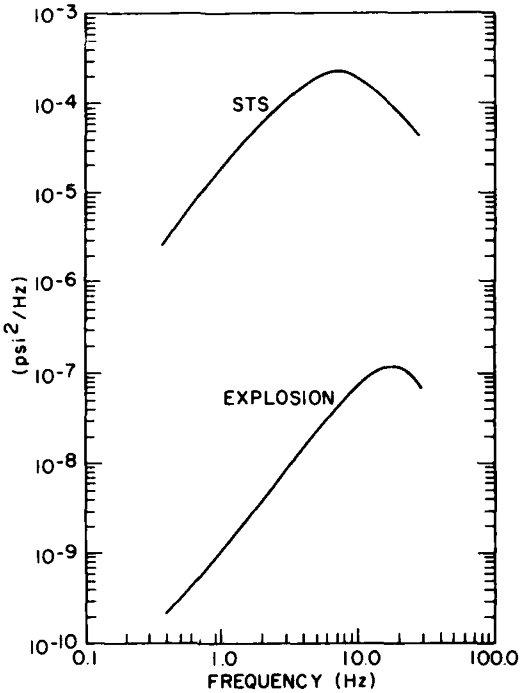


Figure 11. PSD Plot of the STS Acoustic Source at the Time of Peak Pressure Loading and of the 2.3-kg Charge Acoustics Referenced to 300 m

and C2 (see Appendix A) at elevations of 15, 46, and 58 m above the LM, respectively.

Throughout the following discussion, the data exhibited is derived from the launch simulation that produced the maximum rms acceleration for that channel. In general, the waveforms selected represent different launches. The displayed data should not be viewed as the simulation of any single launch. For any given channel, however, all displayed waveforms and spectra are based on one launch simulation. Further, it should be noted that the waveform having the maximum rms acceleration might not produce the most severe environment in terms of any other parameter, such as peak acceleration, velocity, or displacement.

It is appropriate at this time to discuss one restriction on the interpretation of these forecasts. Variations in the peak OASPL of the Shuttle source have not been considered in this model. Thrust augmentation or other factors could affect the peak OASPL as well as the spectral shape of the acoustic emissions. Motions and pressures presented in this report are based on an expected value OASPL for

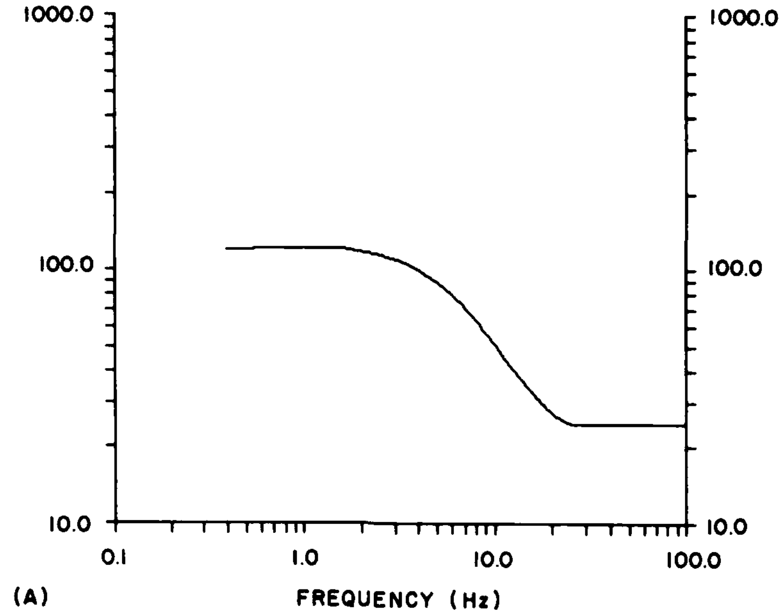


Figure 12a. Spectral Ratio of the STS to Explosion Acoustics for $r_o$ of 300 m

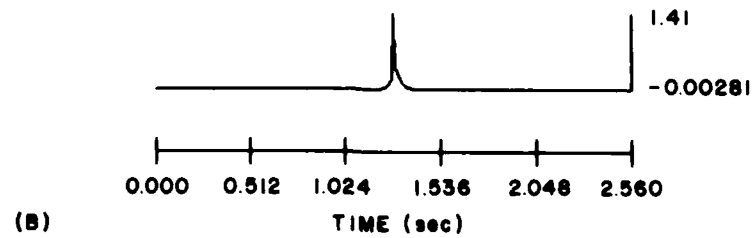


Figure 12b. The Shaping Wavelet, $w(t, r_o)$, for $r_o$ of 300 m

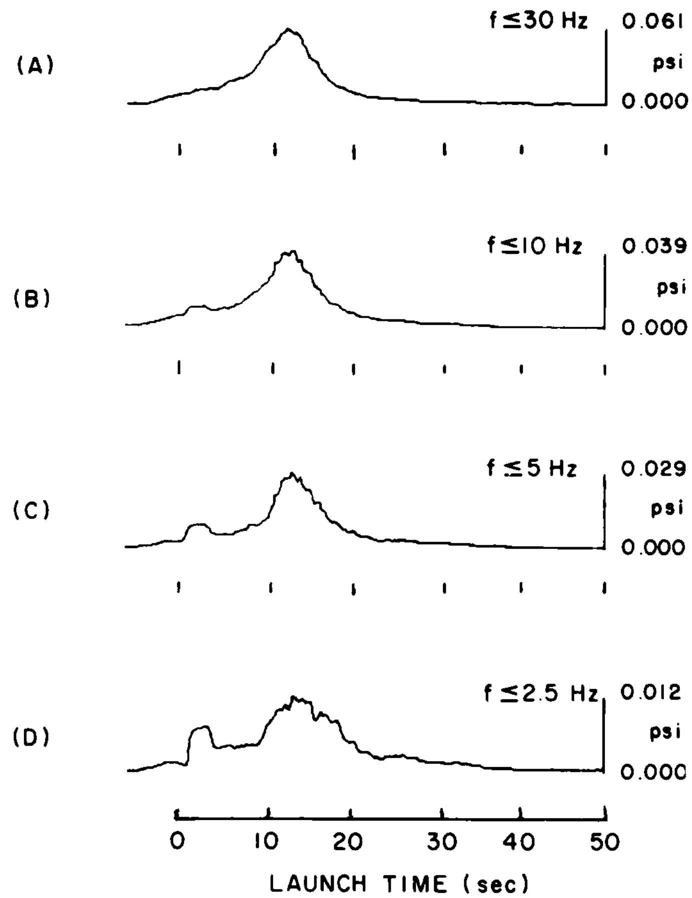


Figure 13. Envelope Functions, $e(t, r_o)$, Determined From STS Mission 41B for 300 m and Using Low Pass Filters With Corners at (a) 30 Hz, (b) 10 Hz, (c) 5 Hz, and (d) 2.5 Hz. The 30-Hz envelope (a) was used for forecasting

a standard Shuttle following a trajectory collocated with the shot points. They can not be considered worst case forecasts.

In Figures 14 through 16, simulated STS launch induced acceleration, and displacement waveforms are shown for each data channel. As stated before, these traces are for the particular launch that produced the maximum rms acceleration for each channel. Maximums, means, and standard deviations of peak acceleration, velocity, displacement, and rms acceleration were evaluated for each channel. These statistics are given in Tables 1 through 4. It is apparent from these figures and tables that the forecast accelerations in the PPR Checkout Cell 2 do not

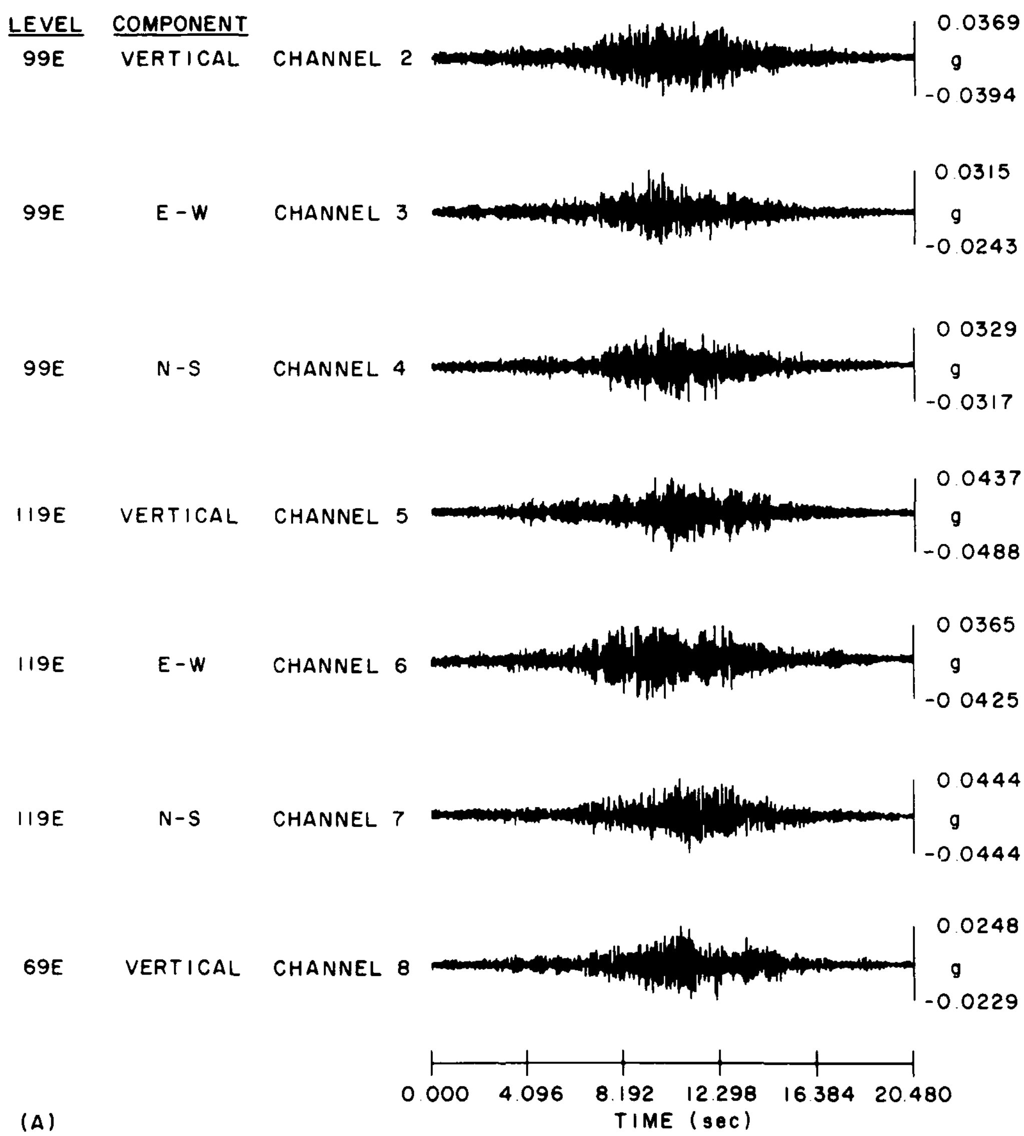


Figure 14. Sample Acceleration Time Series Forecasts for (a) Channels 2 Through 8 and (b) Channels 9 Through 16

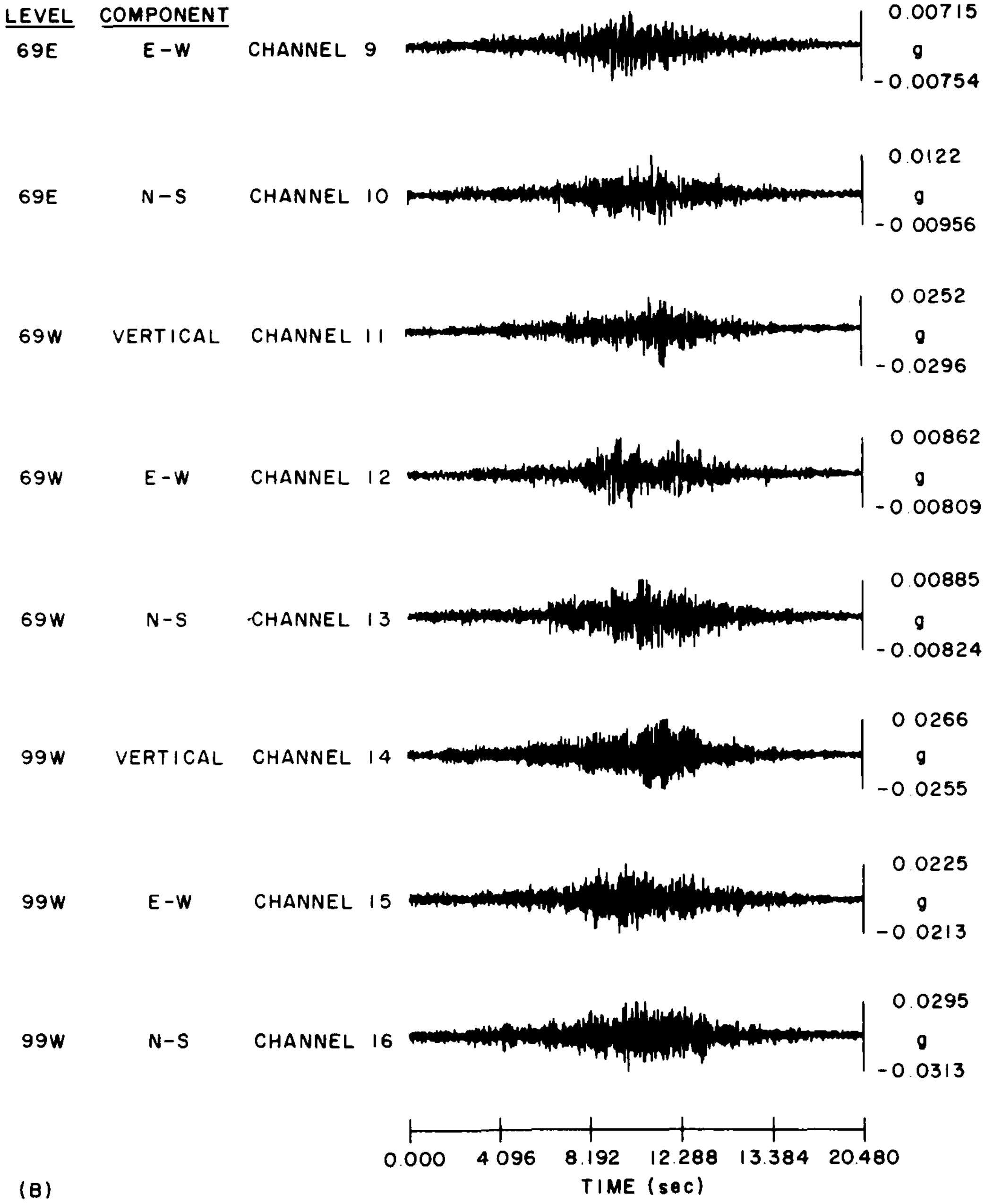


Figure 14. Sample Acceleration Time Series Forecasts for (a) Channels 2 Through 8 and (b) Channels 9 Through 16 (Contd)

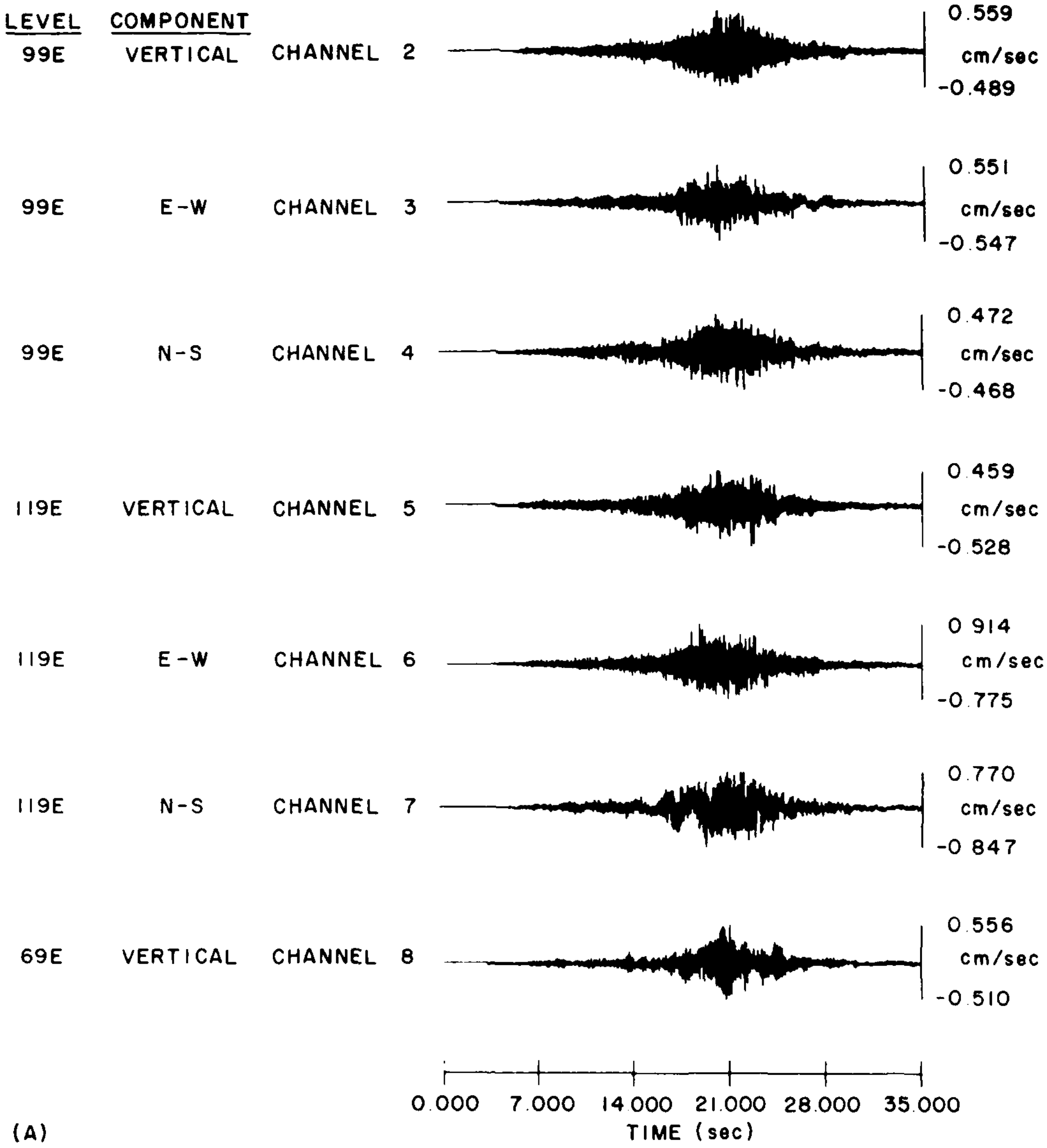


Figure 15. Sample Velocity Time Series Forecasts for (a) Channels 2 Through 8 and (b) Channels 9 Through 16

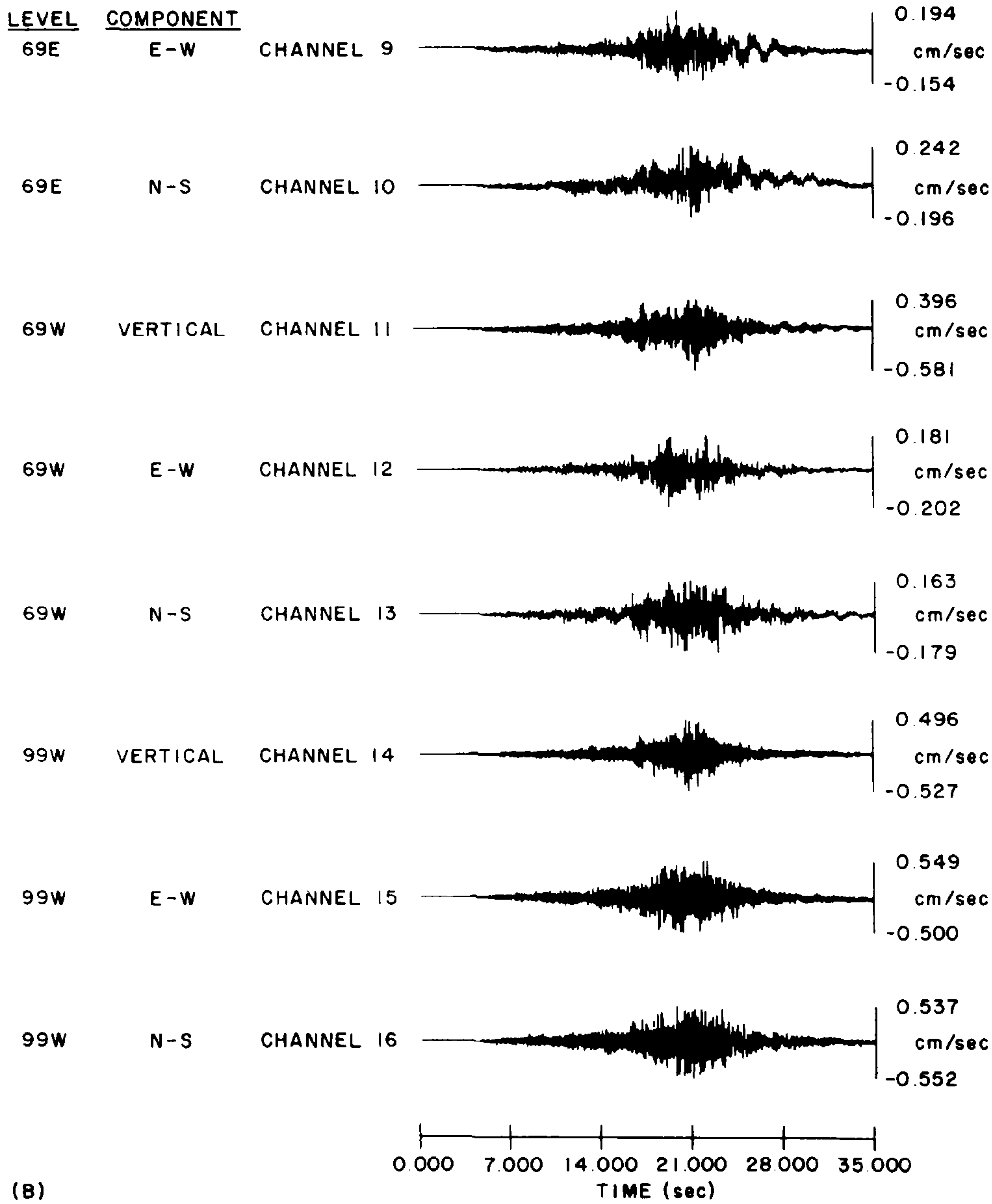


Figure 15. Sample Velocity Time Series Forecasts for (a) Channels 2 Through 8 and (b) Channels 9 Through 16 (Contd)

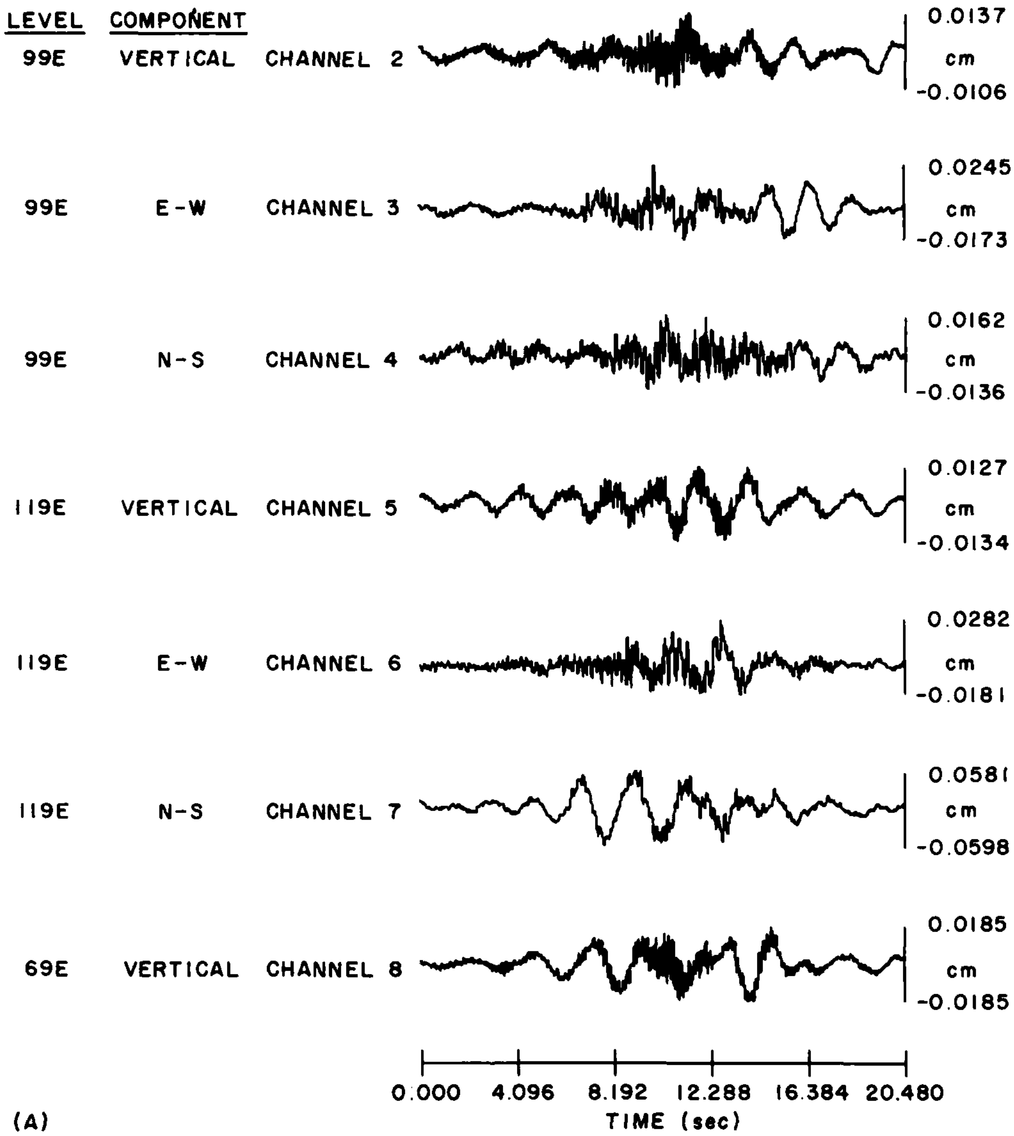


Figure 16. Sample Displacement Time Series Forecasts for Channels 2 Through 8 and (b) Channels 9 Through 16

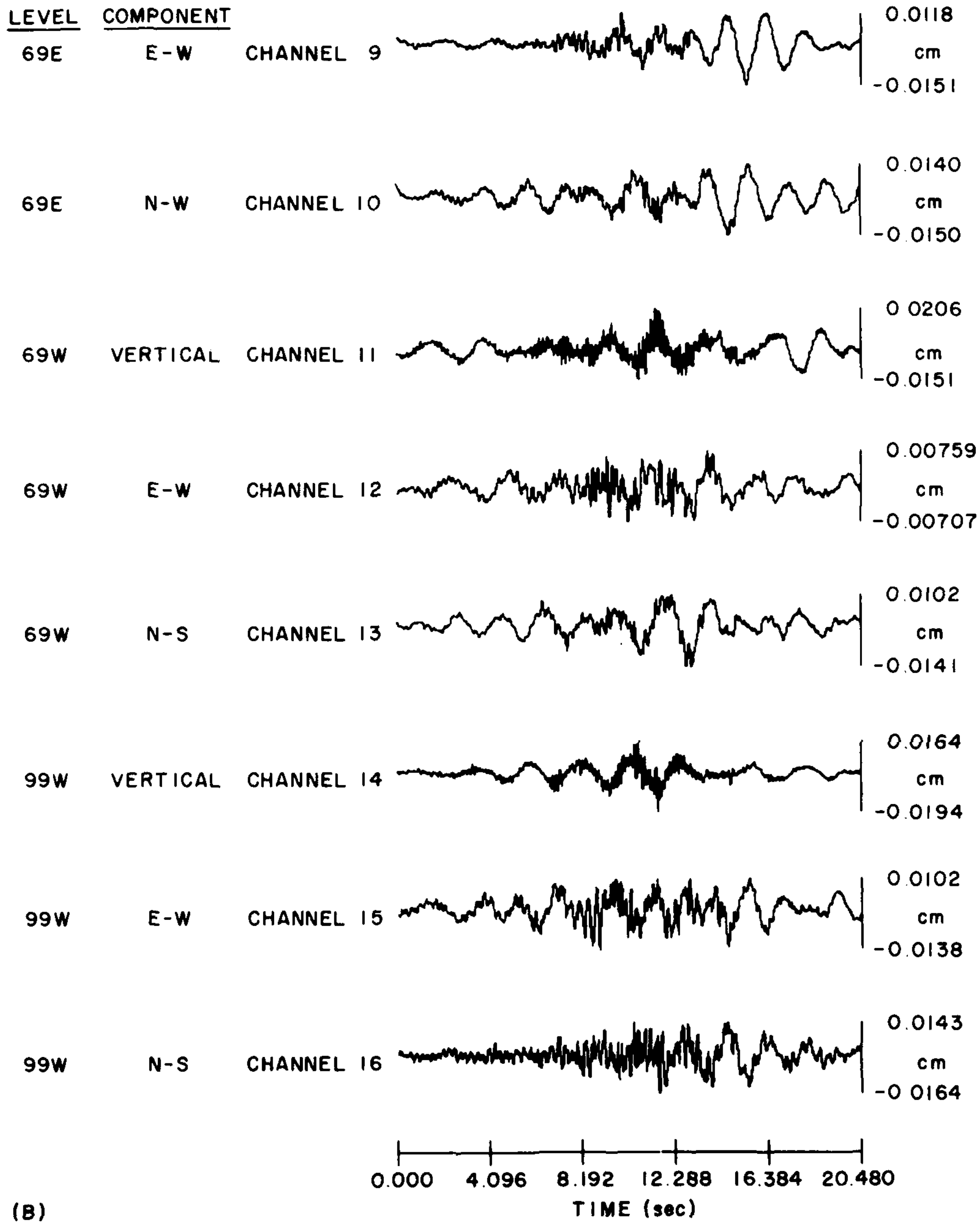


Figure 16. Sample Displacement Time Series Forecasts for Channels 2 Through 8 and (b) Channels 9 Through 16 (Contd)

Table 1. Peak Acceleration Forecast Statistics for the PPR (in g's)

| Ch | Shot A (15 m) | | | Shot B (46 m) | | | Shot C (58 m) | | | 99% Non-exceed. |
|---|---|---|---|---|---|---|---|---|---|---|
| | Maximum | Mean | S. D. | Maximum | Mean | S. D. | Maximum | Mean | S. D. | |
| 2 | 0.0453 | 0.0396 | 0.0047 | 0.0436 | 0.0375 | 0.0036 | 0.0427 | 0.0384 | 0.0036 | 0.0545 |
| 3 | 0.0315 | 0.0275 | 0.0028 | 0.0279 | 0.0250 | 0.0026 | 0.0285 | 0.0241 | 0.0038 | 0.0364 |
| 4 | 0.0352 | 0.0307 | 0.0028 | 0.0329 | 0.0305 | 0.0019 | 0.0348 | 0.0304 | 0.0028 | 0.0395 |
| 5 | 0.0473 | 0.0431 | 0.0036 | 0.0491 | 0.0451 | 0.0026 | 0.0489 | 0.0422 | 0.0057 | 0.0600 |
| 6 | 0.0475 | 0.0433 | 0.0029 | 0.0408 | 0.0361 | 0.0047 | 0.0388 | 0.0320 | 0.0046 | 0.0526 |
| 7 | 0.0496 | 0.0459 | 0.0032 | 0.0469 | 0.0430 | 0.0026 | 0.0531 | 0.0436 | 0.0051 | 0.0595 |
| 8 | 0.0305 | 0.0230 | 0.0052 | 0.0260 | 0.0219 | 0.0028 | 0.0230 | 0.0209 | 0.0018 | 0.0394 |
| 9 | 0.0081 | 0.0071 | 0.0008 | 0.0072 | 0.0066 | 0.0004 | 0.0086 | 0.0064 | 0.0013 | 0.0105 |
| 10 | 0.0099 | 0.0090 | 0.0009 | 0.0131 | 0.0103 | 0.0022 | 0.0127 | 0.0103 | 0.0020 | 0.0171 |
| 11 | 0.0296 | 0.0240 | 0.0035 | 0.0244 | 0.0223 | 0.0023 | 0.0242 | 0.0210 | 0.0031 | 0.0351 |
| 12 | 0.0086 | 0.0072 | 0.0009 | 0.0078 | 0.0070 | 0.0007 | 0.0077 | 0.0067 | 0.0005 | 0.0101 |
| 13 | 0.0098 | 0.0087 | 0.0008 | 0.0124 | 0.0090 | 0.0018 | 0.0134 | 0.0093 | 0.0021 | 0.0159 |
| 14 | 0.0353 | 0.0288 | 0.0062 | 0.0364 | 0.0275 | 0.0044 | 0.0278 | 0.0260 | 0.0018 | 0.0482 |
| 15 | 0.0288 | 0.0234 | 0.0033 | 0.0272 | 0.0225 | 0.0024 | 0.0243 | 0.0208 | 0.0019 | 0.0338 |
| 16 | 0.0377 | 0.0336 | 0.0026 | 0.0325 | 0.0299 | 0.0019 | 0.0311 | 0.0283 | 0.0020 | 0.0417 |

Table 2. Peak Velocity Forecast Statistics for the PPR (in cm/sec)

| Ch | Shot A (15 m) | | | Shot B (46 m) | | | Shot C (58 m) | | | 99% Non-exceed. |
|---|---|---|---|---|---|---|---|---|---|---|
| | Maximum | Mean | S. D. | Maximum | Mean | S. D. | Maximum | Mean | S. D. | |
| 2 | 0.632 | 0.558 | 0.059 | 0.527 | 0.476 | 0.040 | 0.572 | 0.495 | 0.054 | 0.743 |
| 3 | 0.605 | 0.534 | 0.061 | 0.565 | 0.449 | 0.089 | 0.484 | 0.411 | 0.059 | 0.726 |
| 4 | 0.636 | 0.567 | 0.043 | 0.589 | 0.500 | 0.069 | 0.634 | 0.505 | 0.077 | 0.747 |
| 5 | 0.709 | 0.608 | 0.075 | 0.629 | 0.518 | 0.059 | 0.642 | 0.509 | 0.075 | 0.844 |
| 6 | 0.972 | 0.878 | 0.072 | 1.013 | 0.812 | 0.011 | 0.703 | 0.616 | 0.058 | 1.146 |
| 7 | 1.053 | 0.924 | 0.076 | 1.002 | 0.853 | 0.087 | 0.939 | 0.857 | 0.047 | 1.164 |
| 8 | 0.556 | 0.443 | 0.078 | 0.480 | 0.453 | 0.027 | 0.490 | 0.442 | 0.040 | 0.687 |
| 9 | 0.194 | 0.169 | 0.019 | 0.203 | 0.170 | 0.027 | 0.179 | 0.149 | 0.018 | 0.253 |
| 10 | 0.270 | 0.215 | 0.030 | 0.269 | 0.217 | 0.042 | 0.300 | 0.247 | 0.033 | 0.349 |
| 11 | 0.581 | 0.457 | 0.073 | 0.564 | 0.462 | 0.055 | 0.540 | 0.498 | 0.046 | 0.687 |
| 12 | 0.202 | 0.173 | 0.026 | 0.191 | 0.162 | 0.022 | 0.164 | 0.141 | 0.017 | 0.256 |
| 13 | 0.235 | 0.195 | 0.022 | 0.251 | 0.206 | 0.025 | 0.214 | 0.196 | 0.017 | 0.285 |
| 14 | 0.453 | 0.411 | 0.049 | 0.542 | 0.424 | 0.062 | 0.528 | 0.427 | 0.052 | 0.619 |
| 15 | 0.639 | 0.578 | 0.052 | 0.640 | 0.480 | 0.080 | 0.527 | 0.438 | 0.057 | 0.740 |
| 16 | 0.745 | 0.618 | 0.076 | 0.614 | 0.506 | 0.064 | 0.579 | 0.532 | 0.043 | 0.857 |

Table 3. Peak Displacement Forecast Statistics for the PPR (in cm)

| Ch | Shot A (15 m) | | | Shot B (46 m) | | | Shot C (58 m) | | | 99% Non-exceed. |
|---|---|---|---|---|---|---|---|---|---|---|
| | Maximum | Mean | S. D. | Maximum | Mean | S. D. | Maximum | Mean | S. D. | |
| 2 | 0.0254 | 0.0164 | 0.0049 | 0.0205 | 0.0105 | 0.0035 | 0.0299 | 0.0214 | 0.0066 | 0.0422 |
| 3 | 0.0291 | 0.0192 | 0.0063 | 0.0193 | 0.0141 | 0.0030 | 0.0254 | 0.0158 | 0.0057 | 0.0389 |
| 4 | 0.0192 | 0.0169 | 0.0018 | 0.0238 | 0.0201 | 0.0026 | 0.0295 | 0.0215 | 0.0045 | 0.0356 |
| 5 | 0.0203 | 0.0158 | 0.0025 | 0.0215 | 0.0169 | 0.0027 | 0.0172 | 0.0144 | 0.0023 | 0.0254 |
| 6 | 0.0283 | 0.0222 | 0.0035 | 0.0247 | 0.0217 | 0.0023 | 0.0186 | 0.0169 | 0.0012 | 0.0332 |
| 7 | 0.0770 | 0.0530 | 0.0162 | 0.1156 | 0.0682 | 0.0278 | 0.0938 | 0.0661 | 0.0173 | 0.1555 |
| 8 | 0.0284 | 0.0211 | 0.0043 | 0.0163 | 0.0145 | 0.0015 | 0.0243 | 0.0199 | 0.0033 | 0.0346 |
| 9 | 0.0151 | 0.0099 | 0.0026 | 0.0124 | 0.0090 | 0.0023 | 0.0156 | 0.0090 | 0.0037 | 0.0208 |
| 10 | 0.0188 | 0.0156 | 0.0035 | 0.0226 | 0.0164 | 0.0042 | 0.0316 | 0.0205 | 0.0057 | 0.0384 |
| 11 | 0.0312 | 0.0216 | 0.0058 | 0.0201 | 0.0173 | 0.0024 | 0.0308 | 0.0234 | 0.0056 | 0.0409 |
| 12 | 0.0143 | 0.0098 | 0.0024 | 0.0111 | 0.0093 | 0.0018 | 0.0114 | 0.0093 | 0.0019 | 0.0173 |
| 13 | 0.0170 | 0.0123 | 0.0030 | 0.0153 | 0.0130 | 0.0019 | 0.0190 | 0.0154 | 0.0026 | 0.0235 |
| 14 | 0.0154 | 0.0117 | 0.0023 | 0.0134 | 0.0112 | 0.0020 | 0.0197 | 0.0164 | 0.0036 | 0.0278 |
| 15 | 0.0288 | 0.0202 | 0.0052 | 0.0157 | 0.0131 | 0.0016 | 0.0191 | 0.0139 | 0.0027 | 0.0364 |
| 16 | 0.0245 | 0.0199 | 0.0030 | 0.0272 | 0.0221 | 0.0044 | 0.0332 | 0.0240 | 0.0062 | 0.0434 |

Table 4. rms Acceleration Forecast Statistics for the PPR (in g's)

| Ch | Shot A (15 m) | | | Shot B (46 m) | | | Shot C (58 m) | | | 99% Non-exceed. |
|---|---|---|---|---|---|---|---|---|---|---|
| | Maximum | Mean | S. D. | Maximum | Mean | S. D. | Maximum | Mean | S. D. | |
| 2 | 0.0145 | 0.0128 | 0.0014 | 0.0137 | 0.0113 | 0.0014 | 0.0132 | 0.0120 | 0.0012 | 0.0172 |
| 3 | 0.0102 | 0.0085 | 0.0012 | 0.0092 | 0.0078 | 0.0010 | 0.0084 | 0.0078 | 0.0008 | 0.0121 |
| 4 | 0.0110 | 0.0099 | 0.0007 | 0.0117 | 0.0097 | 0.0013 | 0.0111 | 0.0099 | 0.0008 | 0.0136 |
| 5 | 0.0164 | 0.0146 | 0.0014 | 0.0174 | 0.0147 | 0.0016 | 0.0177 | 0.0142 | 0.0018 | 0.0200 |
| 6 | 0.0173 | 0.0142 | 0.0018 | 0.0129 | 0.0117 | 0.0012 | 0.0118 | 0.0105 | 0.0010 | 0.0197 |
| 7 | 0.0160 | 0.0149 | 0.0008 | 0.0165 | 0.0143 | 0.0015 | 0.0163 | 0.0140 | 0.0013 | 0.0189 |
| 8 | 0.0107 | 0.0085 | 0.0018 | 0.0084 | 0.0074 | 0.0010 | 0.0078 | 0.0071 | 0.0007 | 0.0143 |
| 9 | 0.0026 | 0.0024 | 0.0002 | 0.0026 | 0.0022 | 0.0002 | 0.0025 | 0.0020 | 0.0003 | 0.0030 |
| 10 | 0.0038 | 0.0028 | 0.0006 | 0.0039 | 0.0034 | 0.0004 | 0.0040 | 0.0033 | 0.0005 | 0.0049 |
| 11 | 0.0097 | 0.0080 | 0.0010 | 0.0094 | 0.0086 | 0.0008 | 0.0094 | 0.0085 | 0.0010 | 0.0116 |
| 12 | 0.0032 | 0.0024 | 0.0004 | 0.0024 | 0.0021 | 0.0002 | 0.0026 | 0.0021 | 0.0003 | 0.0036 |
| 13 | 0.0031 | 0.0028 | 0.0004 | 0.0037 | 0.0030 | 0.0005 | 0.0035 | 0.0030 | 0.0003 | 0.0045 |
| 14 | 0.0113 | 0.0096 | 0.0014 | 0.0106 | 0.0095 | 0.0007 | 0.0114 | 0.0094 | 0.0013 | 0.0141 |
| 15 | 0.0082 | 0.0075 | 0.0007 | 0.0081 | 0.0075 | 0.0004 | 0.0070 | 0.0066 | 0.0003 | 0.0096 |
| 16 | 0.0135 | 0.0112 | 0.0013 | 0.0099 | 0.0091 | 0.0010 | 0.0104 | 0.0091 | 0.0008 | 0.0154 |

approach either the general vertical or PPR-specific rms acceleration levels of concern. Peak accelerations are more than an order of magnitude below the general level of concern and the rms amplitudes are no more than 4 percent of the 0.5-g level specified for the PPR.

An examination of Tables 1 through 4 indicates that the structural responses of the PPR are only weakly sensitive to source elevation, at least over the range of elevations available to this study. The forecast motions are reasonably stable across the shot heights. For each component of motion, that is, vertical, east-west, and north-south, there is no persistent shift with shot height. It would appear that the assumption of a stationary source location is not unreasonable.

The shot elevations used in this study, however, cover only the first 7 sec of the Shuttle launch trajectory. Considering the cross-sectional area of the PPR exposed to loading, it can be deduced that the PPR will be somewhat underdriven at later times in the trajectory using these shot elevations. This is particularly true when the Shuttle moves well above the main PPR roofline and to the south. This fact will be expanded upon in a later section.

Based on the distribution of the motions parameters from these simulated launches, the 99 percent non-exceedance level for each channel was estimated. This value can be expected to be reached or exceeded in one out of 100 launches. Again, this is not an absolute worst case projection, but assumes mean acoustic emissions from a standard Shuttle source following a typical trajectory. These motion levels were determined by fitting a Gumbel Type I extreme value distribution to the motion levels from the six simulated launches at each shot elevation.[20] Although other distributions were also tested, the Type I distribution provided the best fit to the data. In Tables 1 through 4, the largest estimated 99 percent non-exceedance level using any of the charge heights is stated. Again, these values are well below any established level of concern.

Finally, Figures 17 and 18 show the PSD plots and pseudo-velocity response spectra for each channel based on the launch simulation that produced the maximum rms acceleration. As expected from the rms accelerations, virtually all PSD levels are at least two orders of magnitude below the 0.01 $g^2$/Hz level of concern. Maximum pseudo-velocity responses are all below 10 cm/sec and well below the level of concern taken to be 254 cm/sec.

---

20. Benjamin, J.R., and Cornell, C.A. (1970) Probability, Statistics and Decision for Civil Engineers, McGraw-Hill Book Co., New York.

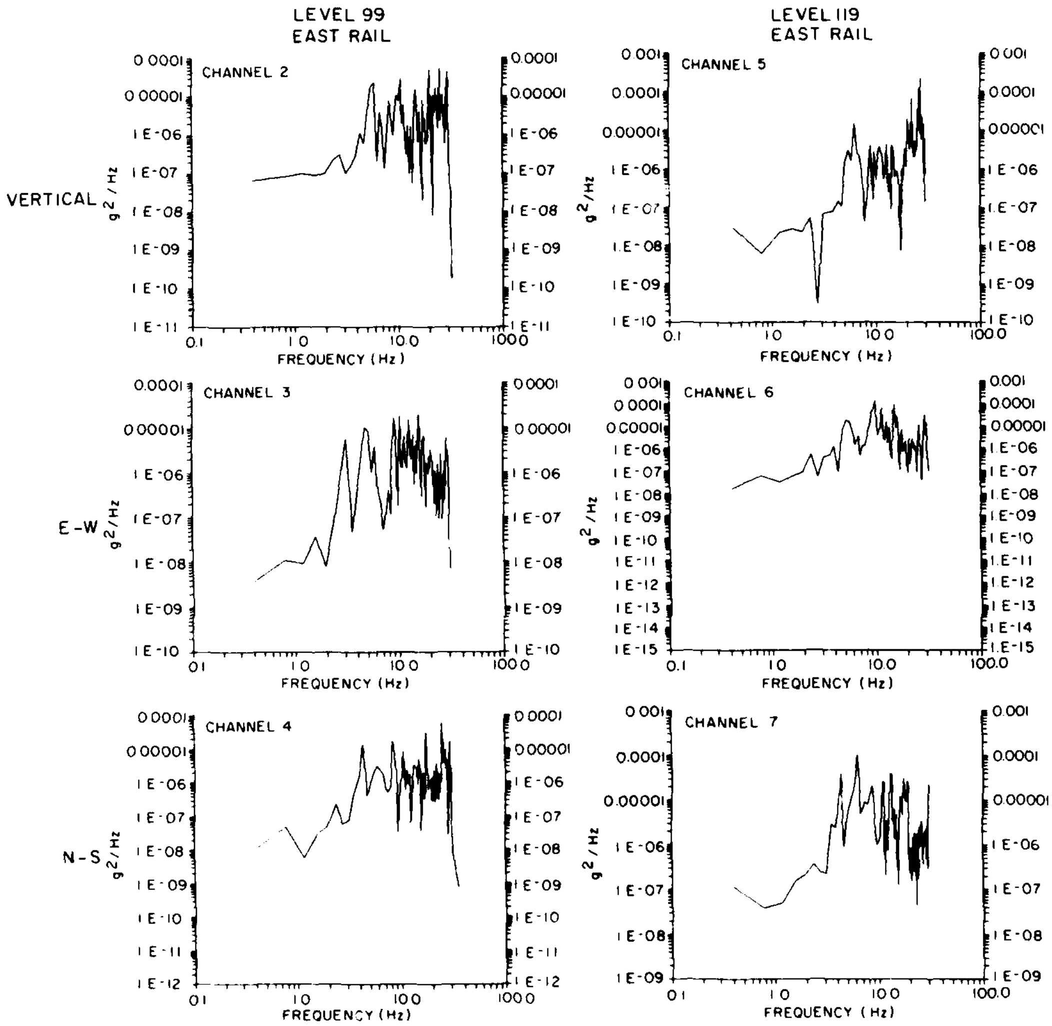


Figure 17. Sample PSD Plots for (a) Levels 99 and 119 East Cell Rail Locations, (b) Level 69 Sensors on the East and West Cell Rail Footings, and (c) Level 99 West Cell Rail Sensors

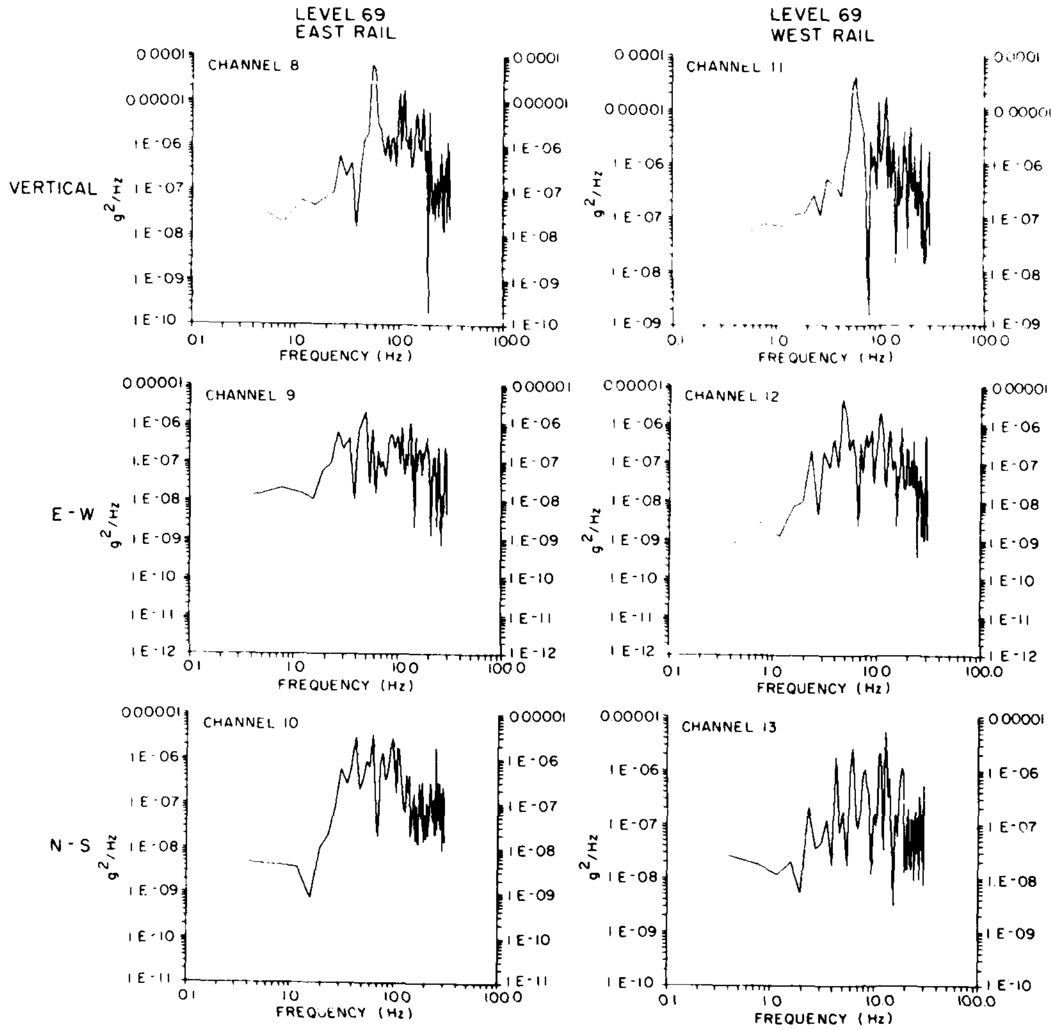


Figure 17. Sample PSD Plots for (a) Levels 99 and 119 East Cell Rail Locations, (b) Level 69 Sensors on the East and West Cell Rail Footings, and (c) Level 99 West Cell Rail Sensors (Contd)

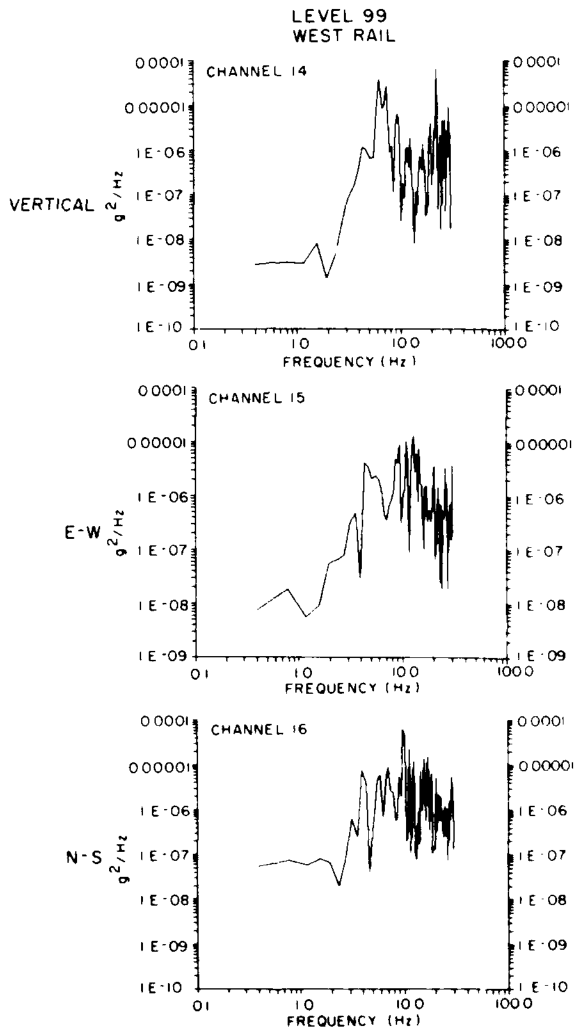


Figure 17. Sample PSD Plots for (a) Levels 99 and 119 East Cell Rail Locations, (b) Level 69 Sensors on the East and West Cell Rail Footings, and (c) Level 99 West Cell Rail Sensors (Contd)

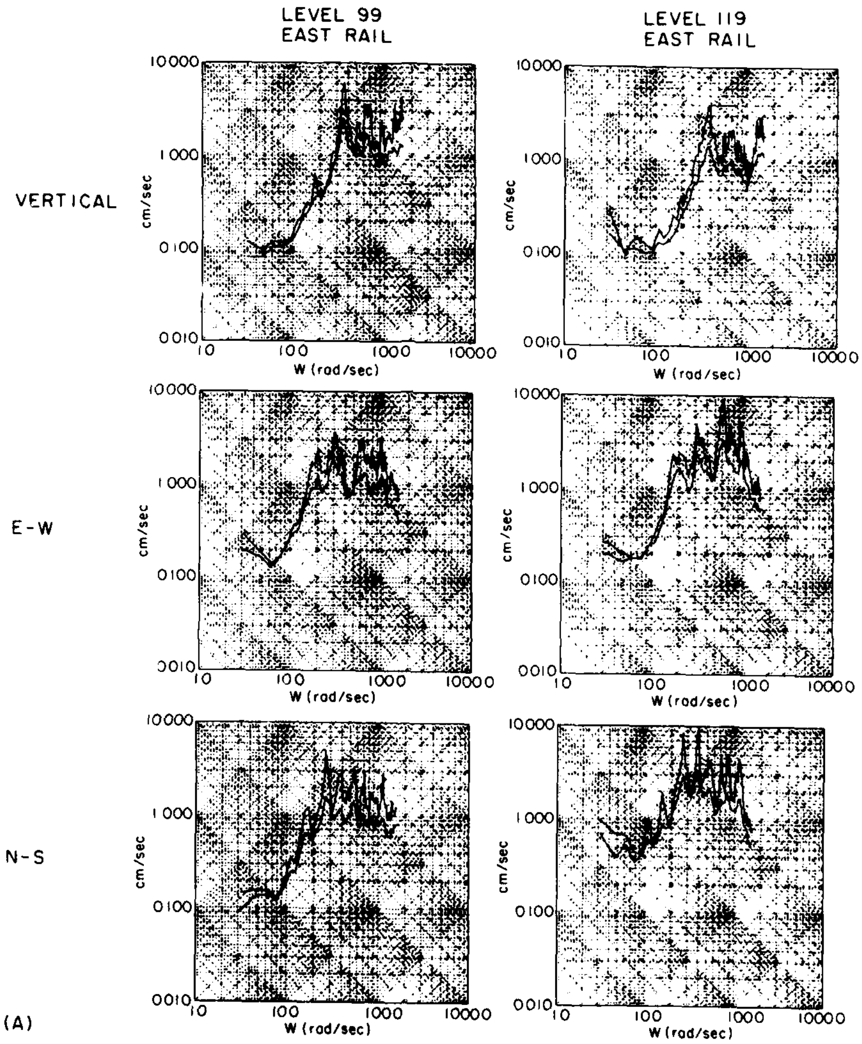


Figure 18. Pseudo-Velocity Response Spectra for Sensors at (a) Levels 99 and 119 on the West Cell Rail, (b) Level 69 on the East and West Cell Rail Footings, and (c) Level 99 on the West Cell Rail

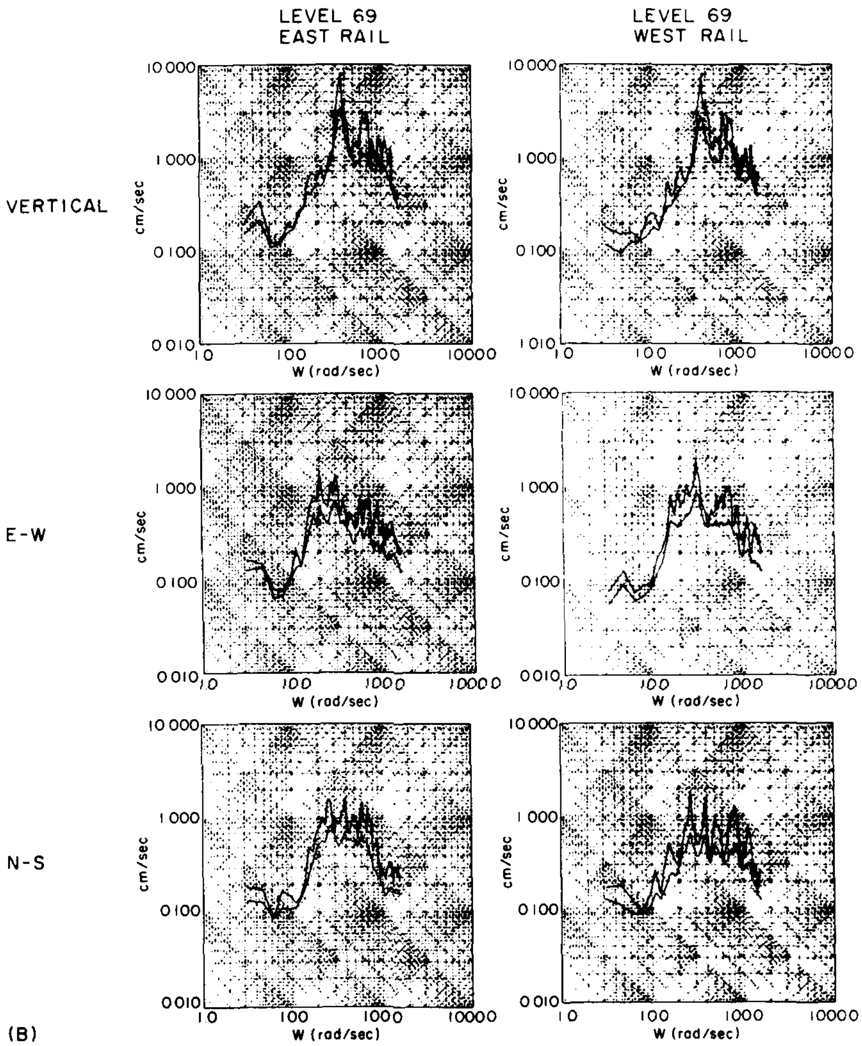


Figure 18. Pseudo-Velocity Response Spectra for Sensors at (a) Levels 99 and 119 on the West Cell Rail, (b) Level 69 on the East and West Cell Rail Footings, and (c) Level 99 on the West Cell Rail (Contd)

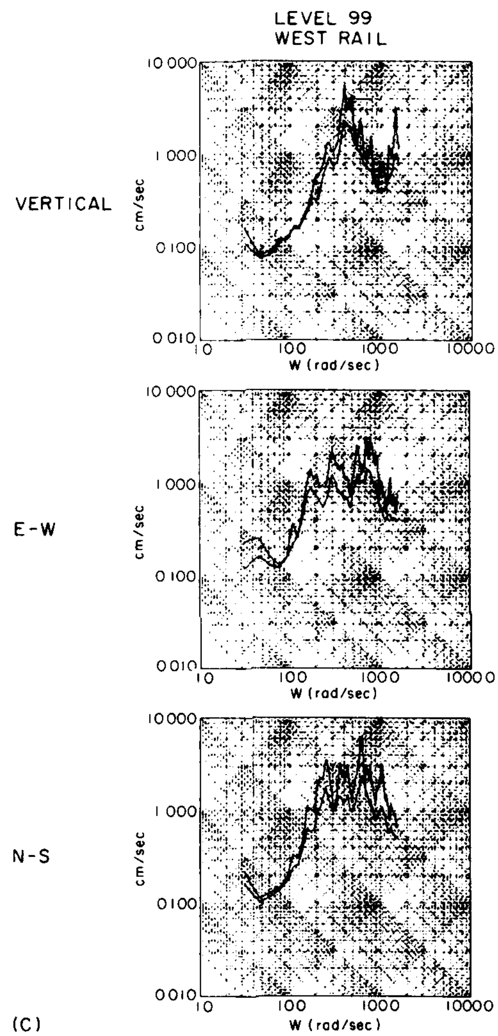


Figure 18. Pseudo-Velocity Response Spectra for Sensors at (a) Levels 99 and 119 on the West Cell Rail, (b) Level 69 on the East and West Cell Rail Footings, and (c) Level 99 on the West Cell Rail (Contd)

### 6.4 Forecast Stability

Some indication of the repeatability of these forecasts can be gained by examining the response functions for each location in the PPR. In Figures 19 and 20, the spectral ratios of the observed motions to the flat-earth acoustics, referenced to 300 m, are shown for channels 2 and 8 for two shots at a height of 46 m. Both channels are vertical seismometers located at Levels 99 and 69, respectively. These spectral ratios are typical of those for all channels and shot elevations. For each channel, the spectral ratios below 30 Hz are essentially the same for both shots. Above 30 Hz differences are noted, but this is above the frequency range of interest in this report. In any case, the differences at high frequencies can readily be explained by slight shifts in the shot location and wind conditions over "like" shots. It can be concluded that, for a given charge elevation, the site responses, including acoustic and seismic propagation properties, have been well established by the AFGL Sounding Program.

In Figures 21 through 23, the average spectral ratios of the observed motions for each shot elevation to the flat-earth acoustics are shown for the three shot elevations on selected channels. These channels are located at Levels 69, 99, and 119, respectively, and are east-west components on the east rail of Checkout Cell 2. Again, they are considered typical examples of all recorded responses. In each case, the major features of the response function spectra remain fairly constant and independent of shot elevation, although there are some relative amplitude changes for individual frequency components. As would be expected from the shot height differences, the spectral ratios from the two higher shots show less variation than does the low shot compared to either of the high shots. Again, for the range of charge elevations used during the Sounding Program, the insensitivity of the PPR responses to source elevation is supported by these figures.

It is unreasonable, however, to expect that this insensitivity will persist after the Shuttle attains a higher elevation and rotates to the south. In particular, it can be assumed that loading on the south face and on the roof of the PPR will increase. Although the level of the acoustics will decrease with increasing range of the Shuttle, the exposed surface area of the PPR will also increase. It is noted that, in launch configuration with the PCR moved back against the PPR, there is roughly four times the unshadowed surface area on the main PPR structure exposed to the south than to the east.

Further analysis of the data provided in Tables 1 through 4 indicates the anticipated effects of a real Shuttle launch. In Figure 24, the mean relative peak displacements on the platforms in the PPR are shown for each component direction. As would be expected, the vertical peak displacements are all much the same along the cell rail. For the horizontal components on the rail, the peak displacements increase with elevation. However, amplification with increasing level is greater

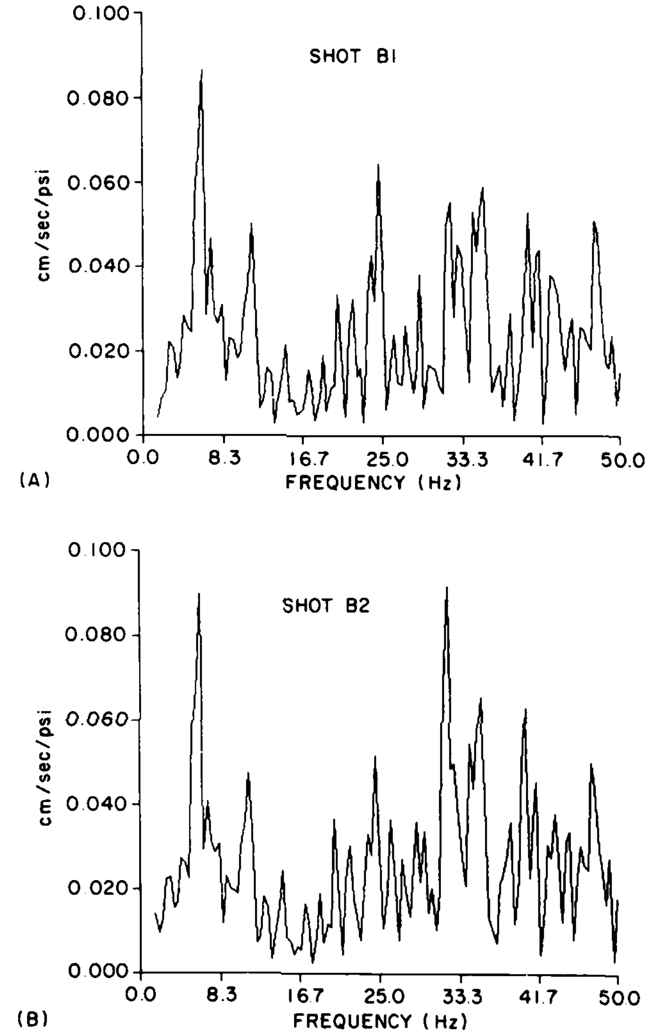


Figure 19. Site-Specific Response Function Spectra for Channel 2 From Shots B1 and B2

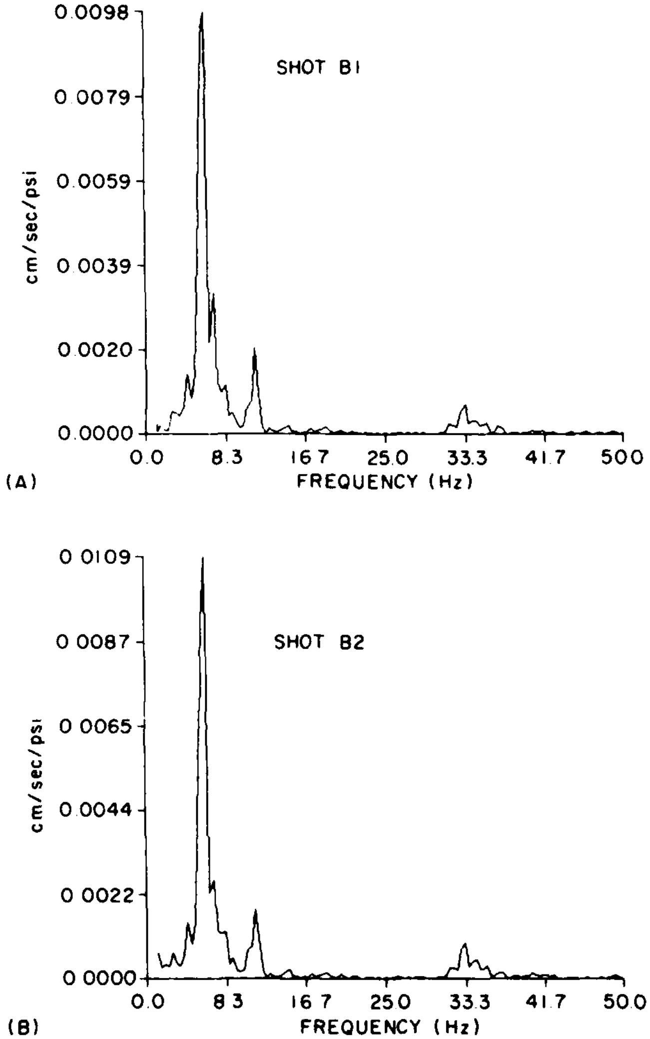


Figure 20. Site-Specific Response Function Spectra for Channel 8 From Shots B1 and B2

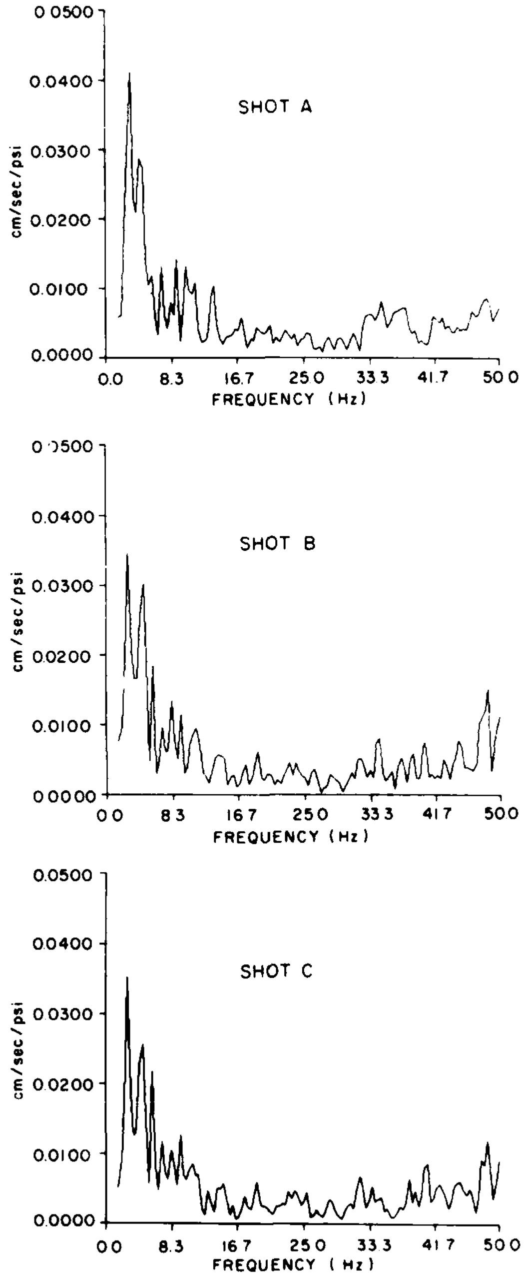


Figure 21. Average Site-Specific Response Function Spectra for Channel 9 for Each Shot Elevation

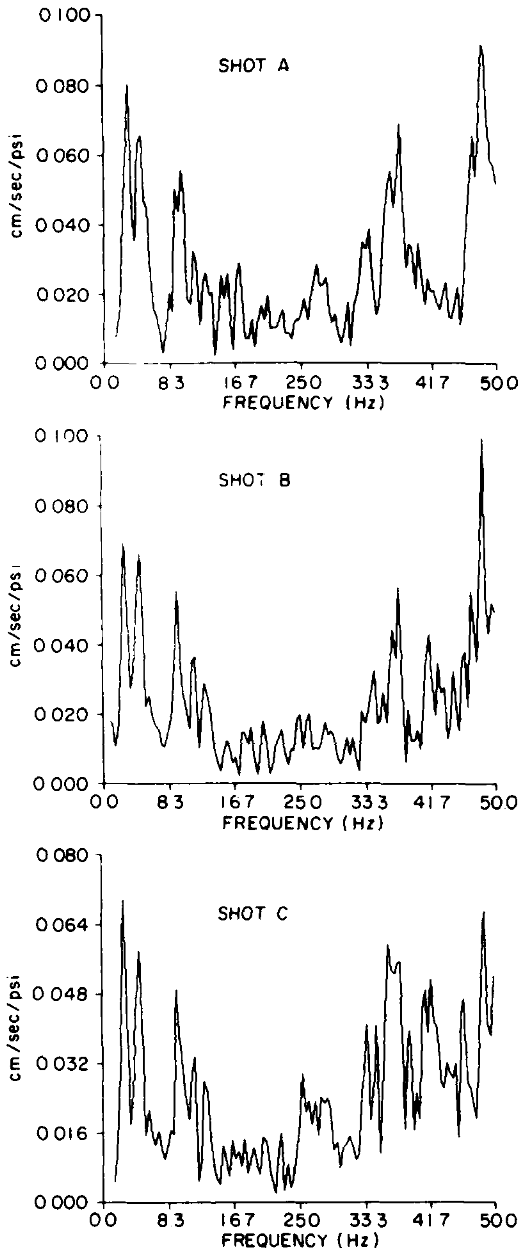


Figure 22. Average Site-Specific Response Function Spectra for Channel 3 for Each Shot Elevation

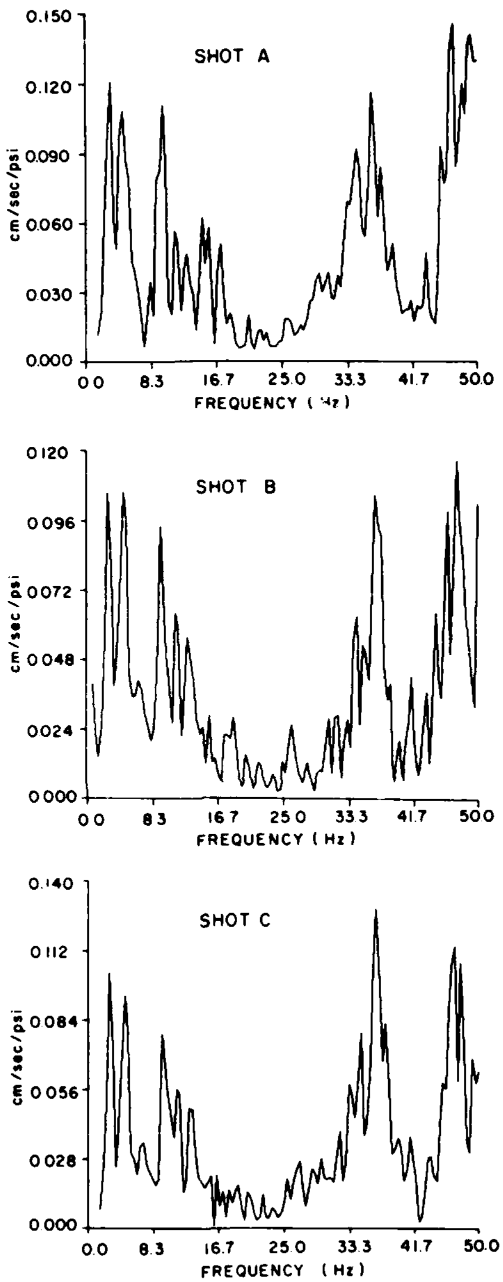


Figure 23. Average Site-Specific Response Function Spectra for Channel 6 for Each Shot Elevation

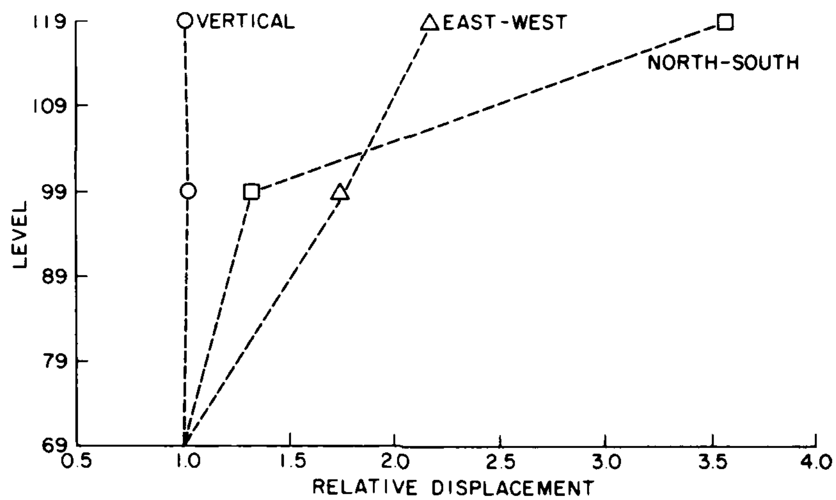


Figure 24. Relative Displacements of the East Rail in Checkout Cell 2 With Elevation in the PPR

above Level 99 in the north-south direction than in the east-west direction. Basically, the PPR is a less rigid structure along it short (north-south) axis than along the long (east-west) axis. It is assumed that the reason this effect occurs above Level 99 is that below this point the PPR is shielded from acoustic loading on the south side by the AB and on the north side by grade. A quick look at Figure 9, the plan view of the PPR, shows that this property is reasonable. Essentially the only north-south shear resistance in the structure is provided by the roof girders and end walls. Along the east-west axis, the checkout cell walls and p forms provide greater stiffness. The lower stiffness in the north-south direction is also reflected by the lower frequency of the fundamental mode in the north-south as compared to east-west direction, 2.76 vs 3.15 Hz, respectively.

Because of the relatively low north-south stiffness and the anticipated load increase on the south face of the PPR, it can be concluded that north-south motions given in this report are underestimated. While it is anticipated that actual launch motions should be higher than the forecast levels, it remains unlikely that the amplification of the motions would be sufficient to approach or exceed the PPR levels of concern.

### 6.5 Seismic Excitation

One question that has been raised throughout the history of the V23 project is the importance of acoustic coupled seismic loading on the motion environments in

structures such as the PPR and LCC. The present data provide some insight to the answer to this question. Distinct seismic excitations were recorded on several channels of output during the AFGL Sounding Program. In Figure 25, the acoustic pressure pulse arrival at channel 1, located 67 m west of the center of the LM, and the seismic arrivals preceding the acoustic excitation are shown for all channels. A simple propagation model is assumed in which the first seismic arrival is generated by the load directly under the shot point and travels through the ground to the PPR. The relative arrival times for the pressure pulse at the channel 1 sensor and the seismic arrival at channel 8, consistently estimate the speed of sound at the time of the shots to be 347 m/sec and the seismic velocity to be 1157 m/sec. The time shift between the arrivals at channels 8 and 11, two vertical seismometers on Level 69, is consistent with this velocity.

Even considering the amplification of the input motions with elevation, for example, channel 6 located at Level 119, the seismic generated motions are no more than 10 percent of the direct acoustic generated motions and are typically much less. In fact, on some channels seismic induced motions are close to ambient noise levels. Neglect of seismic loading is not detrimental to forecasting motion environments in the PPR and LCC using FE models.

### 6.6 Other Studies

One previous study has been made of the launch induced vibration environment in the PPR.[5] This study used an FE model of the PPR and included the effects of thrust augmented Shuttle launch acoustics. None of the reported nodes of the FE model correspond to the locations studied in this report. Yang and Teegarden[5] do, however, state that motions forecast by the FE technique for all three checkout cells were essentially the same. On the basis of this statement, the FE model nodes 275 and 277 correspond with the sensor locations at Levels 99 and 119 of this study. It should be noted that thrust augmentation, as specified by Yang and Teegarden, would produce a frequency dependent amplification of the forecast vibrations when compared to the standard Shuttle configuration used in the present study.[5]

Table 5 provides a comparison of the FE model motions with those obtained in this study. For purposes of comparison, the larger motion forecast for either cell rail was used. Peak, rms, and PSD accelerations from the FE model are, in general, substantially larger than those found by the present analysis. The FE model vertical peak accelerations approach an order of magnitude larger than the equivalent levels forecast in this report.

It appears that the FE model, as was intended, is a conservative estimator of the Shuttle launch induced motions in the PPR.

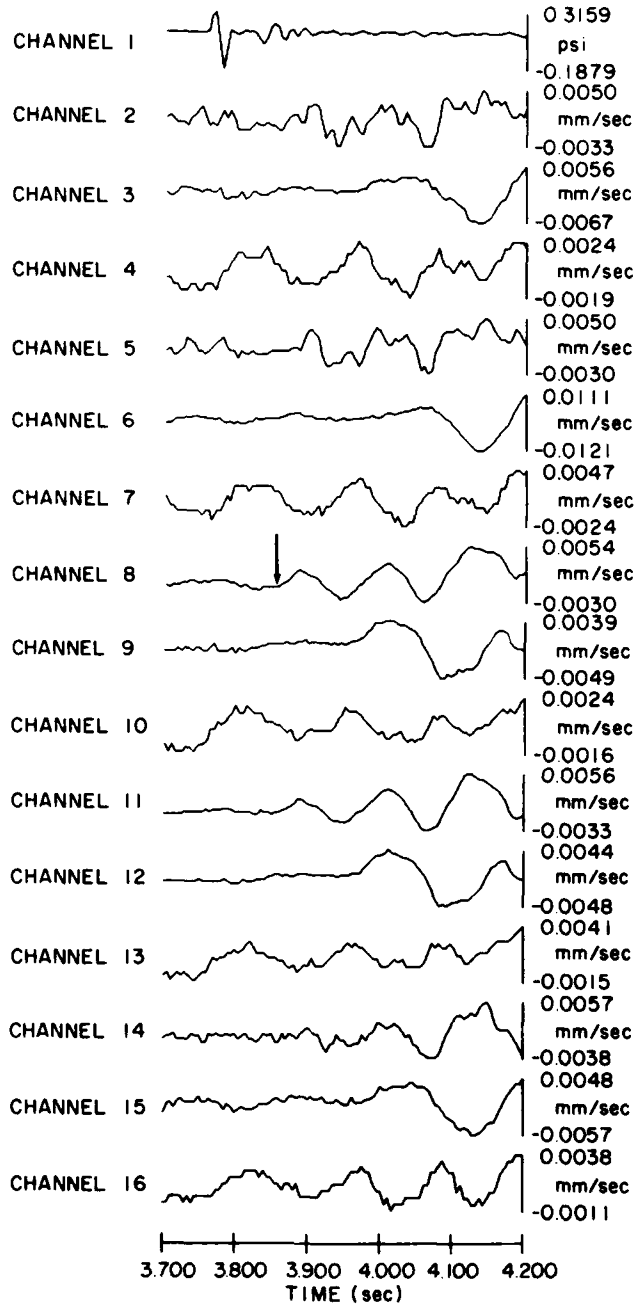


**Figure 25. Pressure Pulse and Seismic Motions Recorded From Shot A2.** (Arrow on channel 8 indicates first seismic arrival)

Table 5. Comparison of FE Model and Present Analysis Forecasts

| Level 99 | Vertical | | E-W | | N-S | |
|---|---|---|---|---|---|---|
| | FE | Present | FE | Present | FE | Present |
| Peak (g's) | 0.2588 | 0.0453 | 0.1023 | 0.0315 | 0.1184 | 0.0377 |
| rms (g's) | 0.0812 | 0.0145 | 0.0286 | 0.0102 | 0.0345 | 0.0135 |
| PSD Peak ($10^{-3}$ $g^2$/Hz) | 1.3543 | 0.0561 | 0.1258 | 0.0235 | 0.0871 | 0.0700 |
| **Level 119** | **Vertical** | | **E-W** | | **N-S** | |
| | FE | Present | FE | Present | FE | Present |
| Peak (g's) | 0.3337 | 0.0491 | 0.0905 | 0.0475 | 0.1266 | 0.0531 |
| rms (g's) | 0.0927 | 0.0177 | 0.0323 | 0.0173 | 0.0383 | 0.0165 |
| PSD Peak ($10^{-3}$ $g^2$/Hz) | 1.7315 | 0.2300 | 0.1161 | 0.1374 | 0.1548 | 0.1273 |

# References


1. Crowley, F. A., and Hartnett, E. B. (1984) Vibro-Acoustic Forecast for Space Shuttle Launches at VAFB, The Payload Checkout Room and the Administration Building, AFGL-TR-84-0322.

2. Crowley, F. A., Hartnett, E. B., and Ossing, H. A. (1983) Amplitude and Phase of Surface Pressure Produced by Space Transportation Systems Mission 5, AFGL-TR-83-0039, AD A125846.

3. Crowley, F. A., Hartnett, E. B., and Fisher, M. A. (1984) Surface Pressure Produced by Space Transportation System Flight 41B, AFGL-TR-84-0213, AD A150793.

4. Martin Marietta Corp. (1980) Payload Requirement Document, VCR-77-081, Rev D.

5. Yang, R. C., and Teegarden, W. T. (1980) Part III, Vibro-Acoustic Study, Payload Preparation Room Summary Report, Martin Marietta Corp., VCR-79-145.

6. Crowley, F. A. (1985) Personal Communication, Boston College.

7. Allen, T. (1982) Launch Induced Environment Data Book, Martin Marietta Corp., VCR-82-293.

8. Battis, J. C. (1979) Seismic Hazards Estimation Study for Vandenberg AFB, AFGL-TR-79-0277, AD A082458.

9. Johnson, D. P. (1985) Comparison of Launch Induced Vibro-Acoustics: Analysis and AFGL Sounding Test, Martin Marietta Corp., Draft Report.

10. (1983) Station Set Specification for VAFB V23 Launch Pad 1 Station Set, Specification No. SSS-2300B, Modification No. 50.

11. Crowley, F. A. (1985) Personal Communication, Boston College.

12. Smith, J. (1985) Personal Communication, Aerospace Corp.

13. Zagzebski, K. P. (1978) Launch Induced Vibro Acoustics Analysis, Launch Control Center, Ralph M. Parsons Co., TOR No. 114.

14. Wheeler, R.H., and Teegarden, W.T. (1982) Launch Induced Vibration Assessment, Final Report, Martin Marietta Corp., *VCR-82-337*.

15. NASA (1976) Environment and Test Specification Levels: Ground Support Equipment for Space Shuttle System Launch Complex 39, Acoustic and Vibration, Vol. I, GP-1059, Rev A.

16. Jenkins, G.M., and Watts, D.G. (1969) Spectral Analysis and Its Applications, Holden-Day, San Francisco.

17. Crowley, F.A., Hartnett, E.B., and Ossing, H.A. (1980) The Seismo-Acoustic Disturbance Produced by a Titan III-D With Application to the Space Transportation System Launch Environment at Vandenberg AFB, AFGL-TR-80-0358, AD A100209.

18. Powell, A. (1964) Theory of vortex sound, J. Acoust. Soc. Am. 36:177-195.

19. Robinson, E.A. (1967) Statistical Communication and Detection, Griffin, London.

20. Benjamin, J.R., and Cornell, C.A. (1970) Probability, Statistics and Decision for Civil Engineers, McGraw-Hill Book Co., New York.

# Appendix A

## AFGL Sounding Program

The AFGL Sounding Program was designed to measure pressures and vibrations produced on major GSS facilities at V23 by small explosive detonations over the LM. This effort was one of a series of SD sponsored studies intended to upgrade the vibro-acoustic forecasts for STS launches at the VAFB facility. The program was planned as a two phase study in which the first stage called for a limited effort, primarily intended to develop coordination between the numerous groups that were required to run the experiment. The second phase was to be a production effort involving a much greater number of sensor locations and charge detonations.

In April 1984, SATAF reconsidered the need to conduct the second phase and, subsequently, Phase II was formally cancelled in August 1984. As a consequence, vibro-acoustic forecasts for V23, of necessity, have been restricted to those sensor locations used during the preliminary study of March, 1984.

On the mornings of 16 and 17 March 1984, a total of 13 charges were detonated over the LM at V23 and the induced motions were recorded at various locations on V23. Coverage during these shots was essentially restricted to the PPR, PCR, and AB. All V23 structures were in launch configuration during these tests. However, construction had not been completed on all facilities. The major construction work remaining at that time was the installation of roof and wall panels on the SAB. Completion of this work can only intensify reverberations observed during the Sounding Program.

The shots were located at three elevations above the LM, at 15, 46, and 58 m. Two detonations were made at each elevation. Throughout this report these shot elevations are referred to as Shots A, B, and C, respectively. These elevations cover the first 7 sec of a shuttle trajectory. The distribution was limited by the height of a line connecting the SAB and the MST roofs, from which the charges were elevated. The original plan called for higher shot elevations using a tethered balloon to suspend the charges. Due to interference from construction equipment on the pad and high winds, however, all attempts to launch the balloon were aborted and the suspended line was substituted.

Measurements were taken by an element of the AFGL Geophysical Data Acquisition System (GDAS). Individual channel responses were determined by analyzing the transients excited by a step input, with all sensors in place, just before and following the shots for that day. Channel scale factors are traceable to a force produced by a proof mass for seismometers, or a pressure developed by a column of water of known height for pressure transducers. Noise is dominated by ambient conditions with inconsequential system noise.

For the 16 March shot sequence, the GDAS was installed in the PPR Checkout Cell 2 with 15 seismometers and one reference pressure transducer located near the LM. On 17 March the sensor configuration was changed and the sensors were placed in the PCR and AB. Information on the system configuration for the second shot sequence is given by Crowley and Hartnett.[A1] Table A1 and Figure A1 give the locations of all sensors used during the PPR study. Figure A2 gives the system responses for each channel. It should be noted that the gains for channels 8 through through 13 were increased by a factor of 2.25 after the first shot, shot A1. The system response functions are given for the system configuration after this gain change.

For each shot elevation, 15, 46, and 58 m, two separate charges were detonated and the motions recorded. The measured vibration and pressure wavelets for each shot and location are shown in Figures A3 through A8. These wavelets establish the site-specific vibration responses to acoustic loading for a source located at the three points along the STS launch trajectory. Each shot in this sequence was 2.3 kg of C4 explosive.

---

A1. Crowley, F.A., and Hartnett, E.B. (1984) Vibro-Acoustic Forecast for Space Shuttle Launches at VAFB, The Payload Checkout Room and the Administration Building, AFGL-TR-84-0322.

Table A1. Sounding Test Channel Identification (PPR)

| Channel | Sensor | Component | Location |
|---|---|---|---|
| 1 | pressure | ---- | 50 m west of Launch Mount |
| 2 | seismometer | vertical | Level 99 - east rail |
| 3 | seismometer | east-west | Level 99 - east rail |
| 4 | seismometer | north-south | Level 99 - east rail |
| 5 | seismometer | vertical | Level 119 - east rail |
| 6 | seismometer | east-west | Level 119 - east rail |
| 7 | seismometer | north-south | Level 119 - east rail |
| 8 | seismometer | vertical | Level 69 - east rail |
| 9 | seismometer | east-west | Level 69 - east rail |
| 10 | seismometer | north-south | Level 69 - east rail |
| 11 | seismometer | vertical | Level 69 - west rail |
| 12 | seismometer | east-west | Level 69 - west rail |
| 13 | seismometer | north-south | Level 69 - west rail |
| 14 | seismometer | vertical | Level 99 - west rail |
| 15 | seismometer | east-west | Level 99 - west rail |
| 16 | seismometer | north-south | Level 99 - west rail |

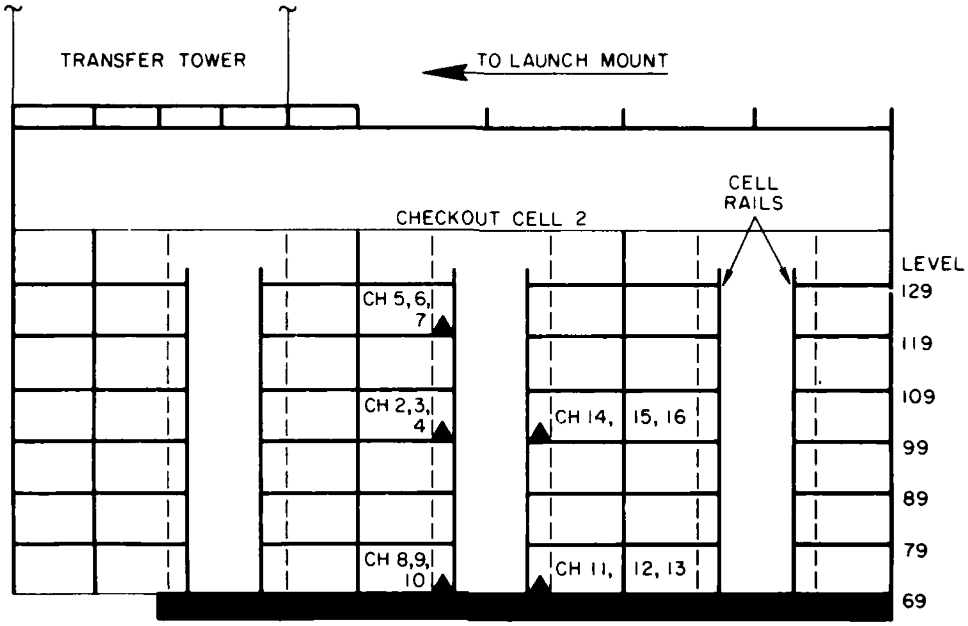


Figure A1. Cross-Section of PPR Showing Sensor Locations

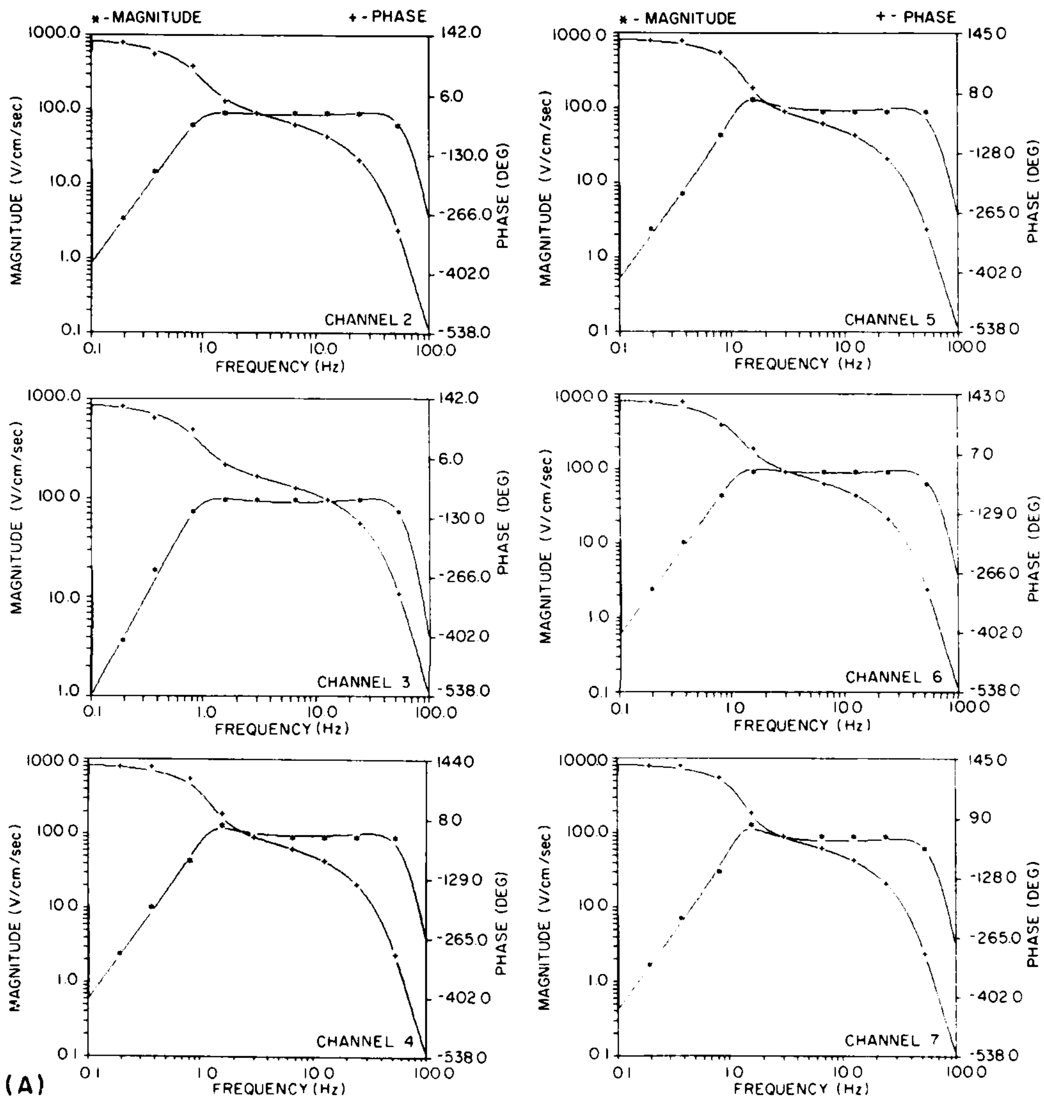


Figure A2. System Response Curves for (a) Channels 2 through 7, (b) Channels 8 Through 13, and (c) Channels 14 Through 16

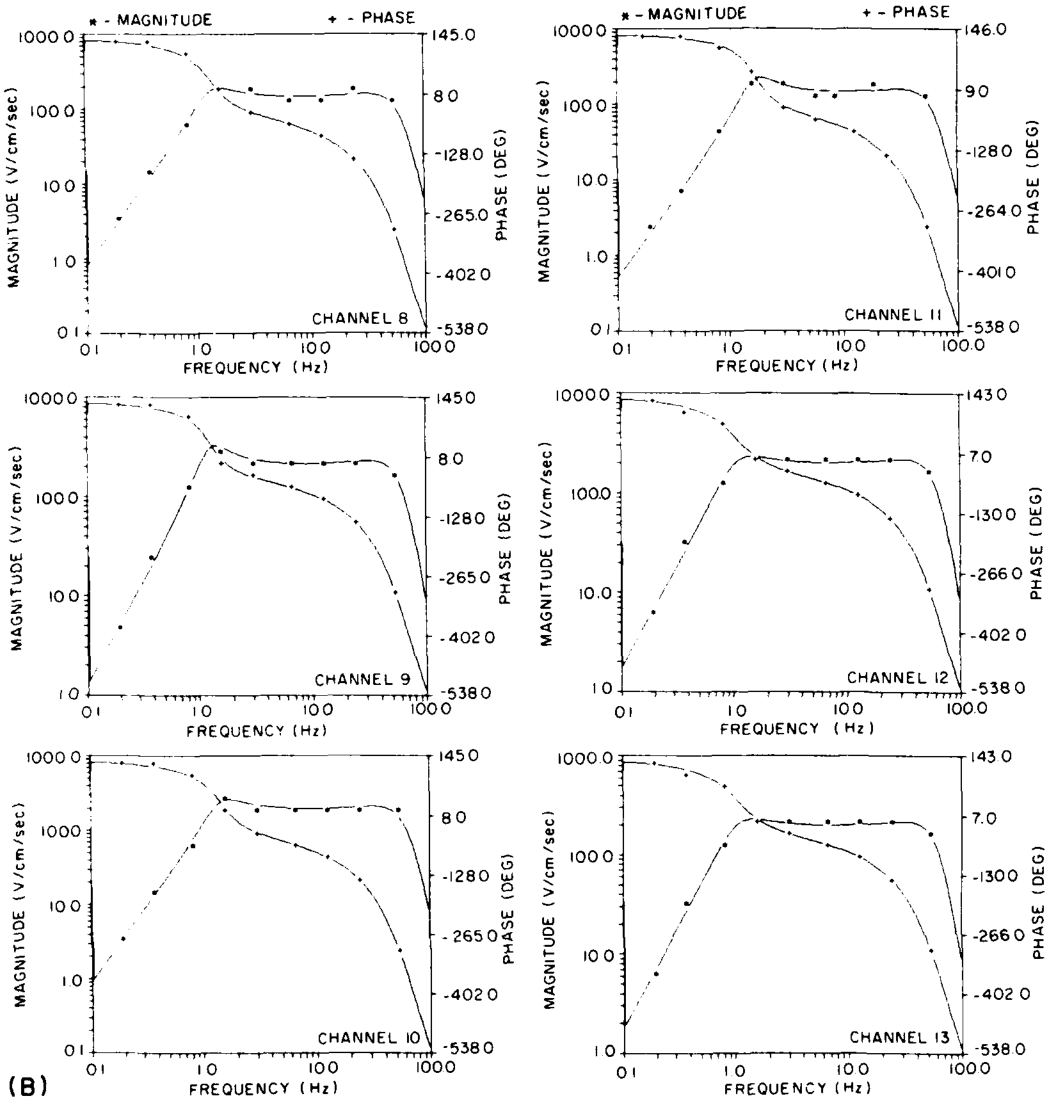


Figure A2. System Response Curves for (a) Channels 2 Through 7, (b) Channels 8 Through 13, and (c) Channels 14 Through 16 (Contd)

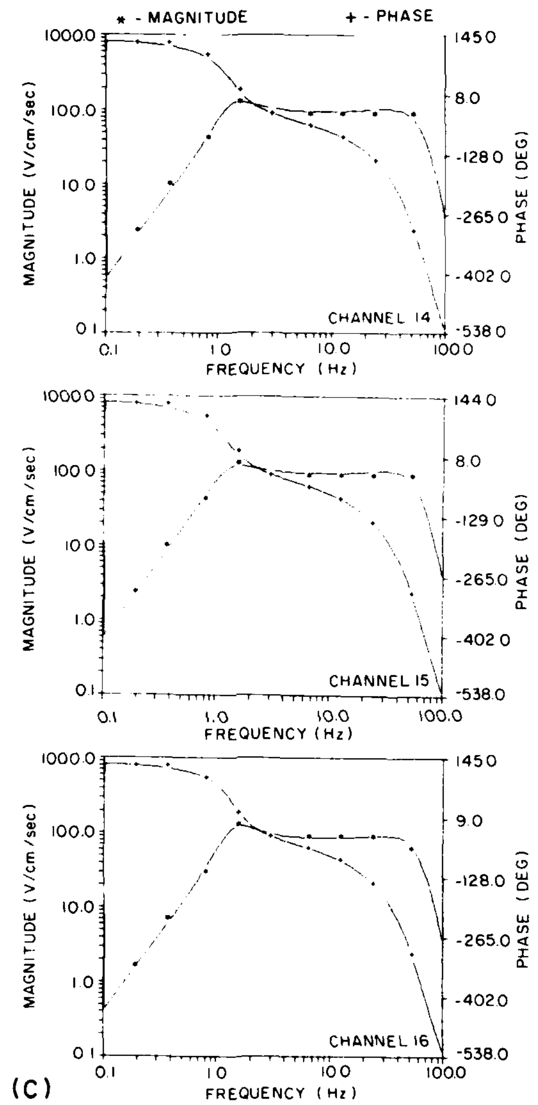


(C)

Figure A2. System Response Curves for (a) Channels 2 Through 7, (b) Channels 8 Through 13, and (c) Channels 14 Through 16 (Contd)

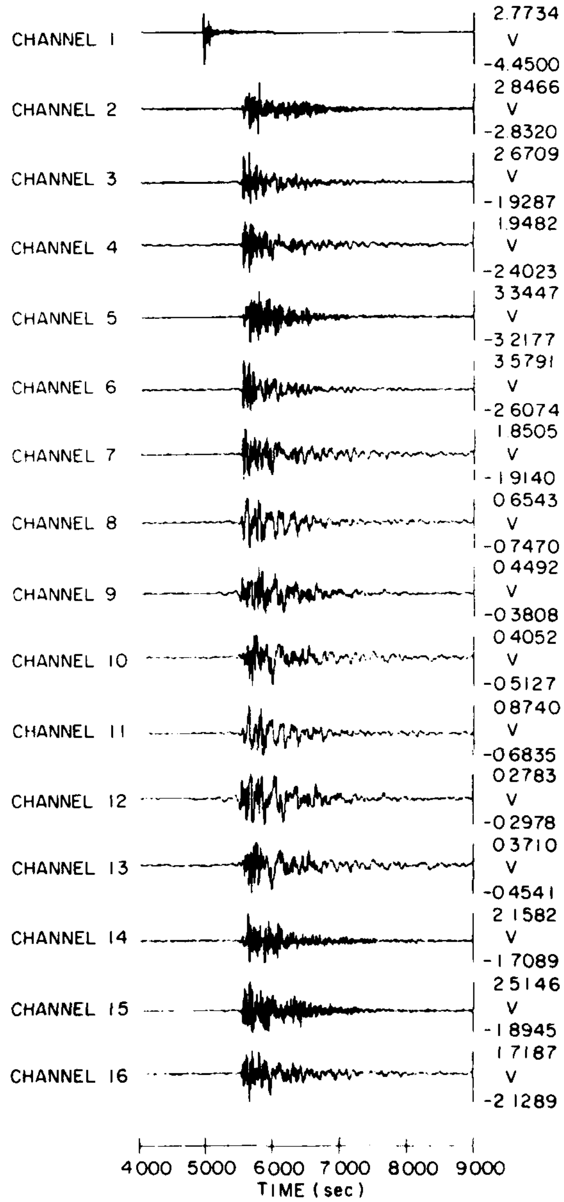


Figure A3. Raw Data Traces for Shot A1

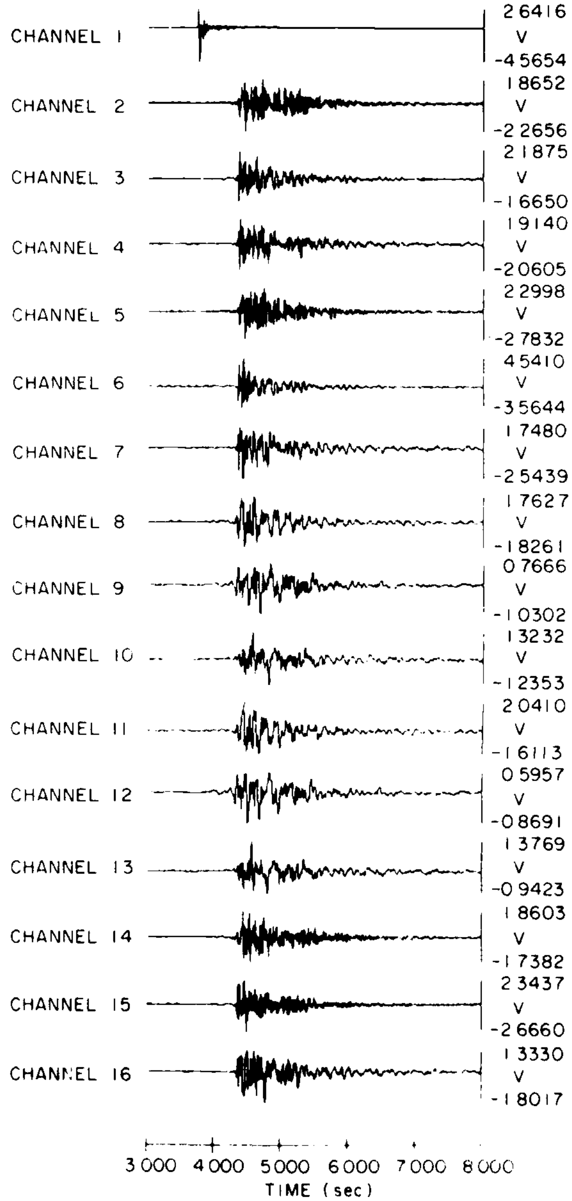


Figure A4. Raw Data Traces for Shot A2

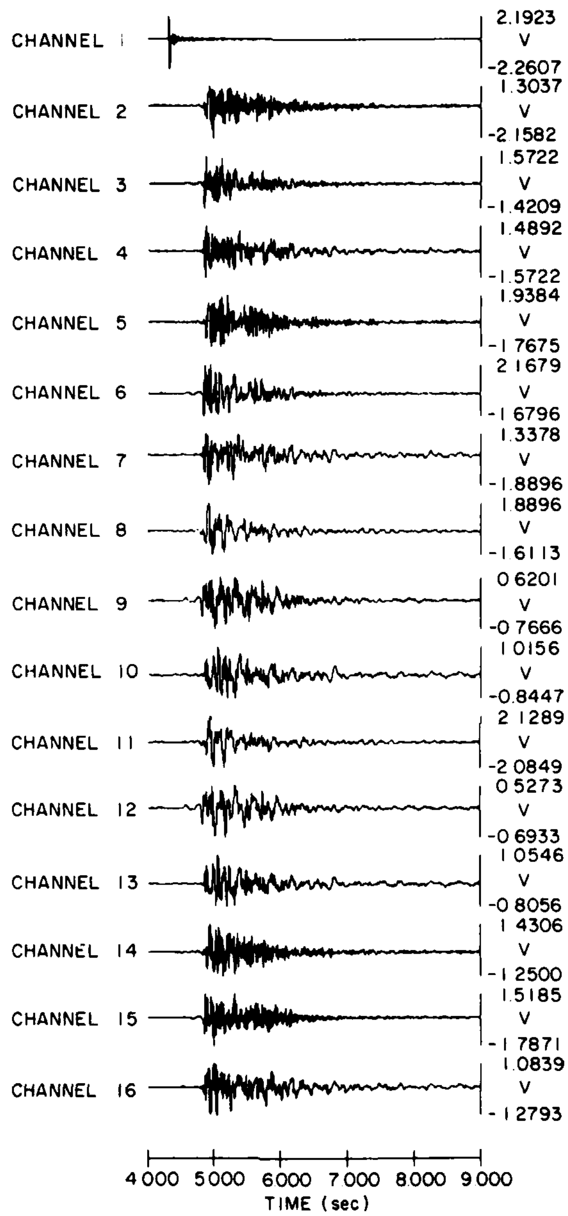


Figure A5. Raw Data Traces for Shot B1

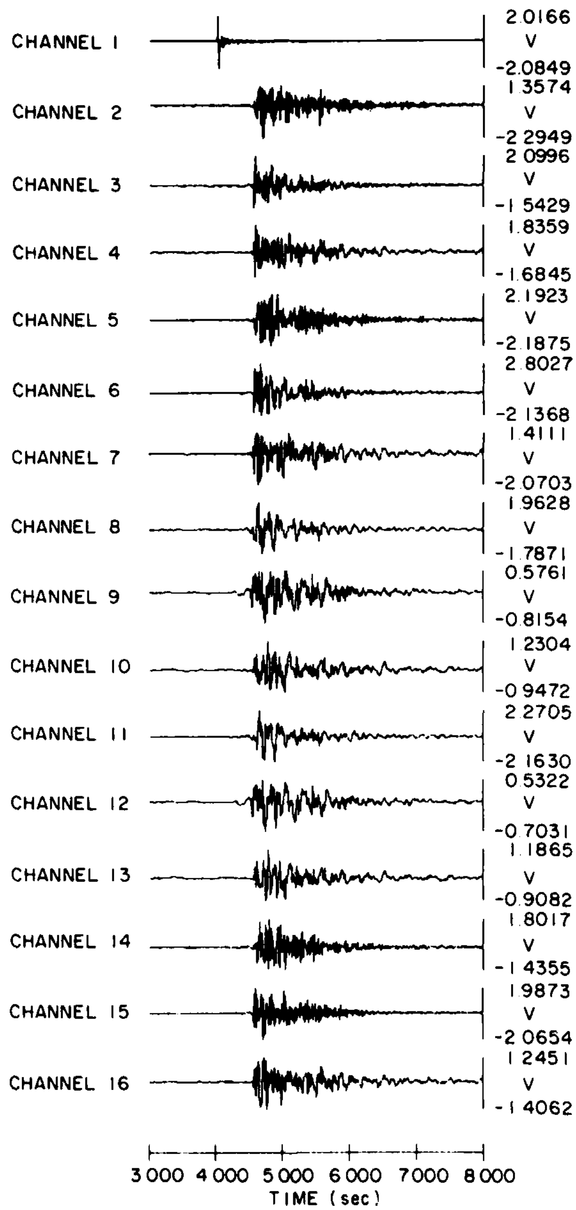


Figure A6. Raw Data Traces for Shot B2

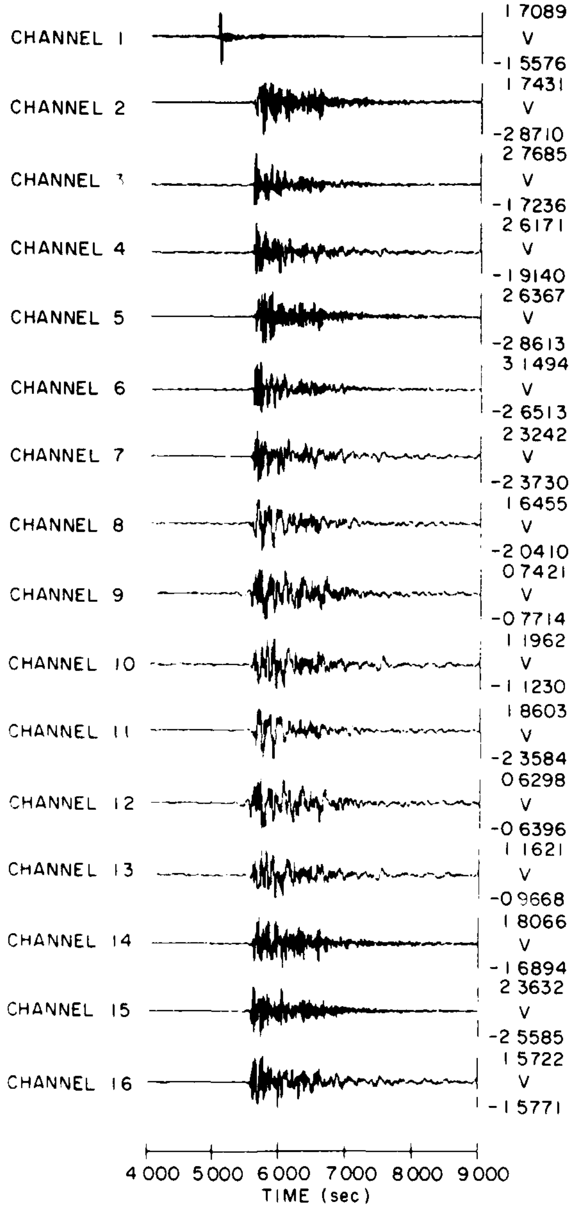


Figure A7. Raw Data Traces for Shot C1

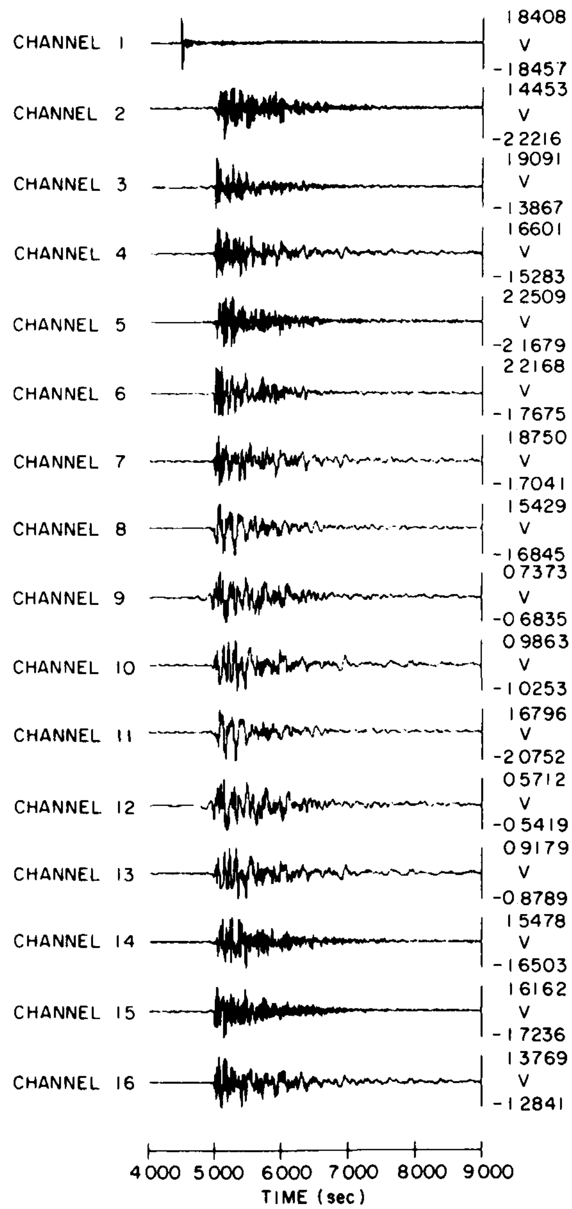


Figure A8. Raw Data Traces for Shot C2

# Appendix B

## Flat-Earth Vibro-Acoustics

### B.1 SHUTTLE SOURCE SPECTRUM

Previous studies have shown that the acoustic emissions of the STS propulsion system can be modeled as an equivalent point source having the spectral attributes described by the theoretical form proposed by Powell for undeflected, plume generated acoustics.[B1-B3] This holds for observations made in a far-field, flat-earth location, such as at KSC, and for times around peak pressure loading. The spectral form of the STS acoustic source is given by

$$G^{STS}(f, r_o) = [(4Q(r_o)/\pi f_m(r_o)][\{f/f_m(r_o)\} + \{f_m(r_o)/f\}]^{-2} \quad ,$$

where f is frequency, $Q(r_o)$ is the OASPL about the time of peak loading, and $f_m(r_o)$ is the frequency of the spectral maximum. The values of $f_m(r_o)$ and $Q(r_o)$ used for this study were 7.25 Hz and 147.6 dB. These values were based on STS

---

B1. Crowley, F.A., Hartnett, E.B., and Ossing, H.A. (1983) Amplitude and Phase of Surface Pressure Produced by Space Transportation Systems Mission 5, AFGL-TR-83-0039, AD A125846.

B2. Crowley, F.A., Hartnett, E.B., and Fisher, M.A. (1984) Surface Pressure Produced by Space Transportation System Flight 41B, AFGL-TR-84-0213, AD A150793.

B3. Powell, A. (1964) Theory of vortex sound, J. Acoust. Soc. Am. 36:177-195.

Mission 41B acoustic data. A plot of the resulting STS source spectrum, referenced to 300 m, is given in Figure 11 of the main text.

## B.2 EXPLOSIVE SOURCE MODEL

Pressure wavelets produced by a 2.3 kg charge were measured at the Explosive and Ordnance Disposal (EOD) Test Range at VAFB. The range is a flat area largely free of surface obstacles. Boundary acoustics at this site were taken to be much the same as those for Pad 39A at KSC. Differences between the pressure measurements of Shuttle launches at KSC and charge detonations at the EOD site, at the same range, were taken to be attributable to the sources alone.

Figure B1 shows the pressure sensor locations during the EOD Test Range detonations and Figure B2 shows the pressure recordings of the 2.3 kg charge detonation. It can be seen that the pulse propagates over the array without change in form, a characteristic of spherical, far-field acoustics. Each of these wavelets is a representation of the explosion source wavelet, $g^E(t, r_o)$, for a reference range equal to the source to sensor range. The mean phase velocity for the detonations was 344 m/sec, as seen in Figure B3. The explosion source spectrum is given in Figure 11 of the main text.

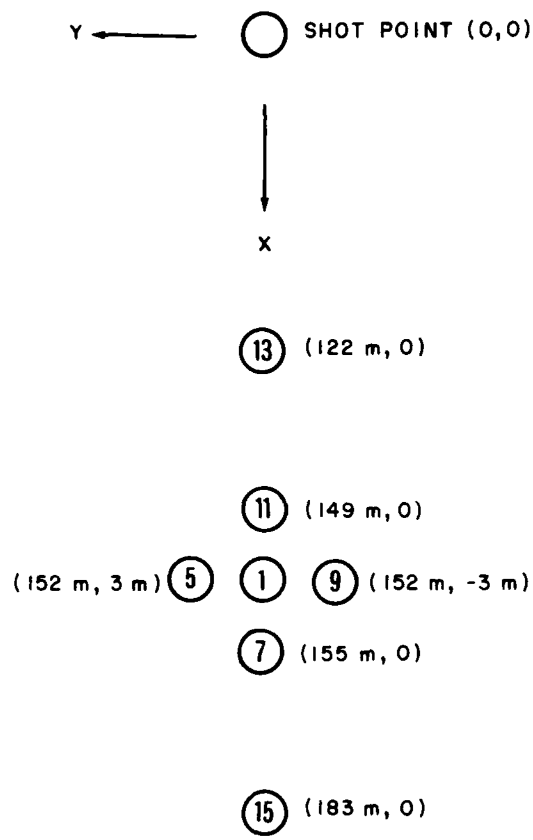


Figure B1. Pressure Sensor Configuration for EOD Range Shots

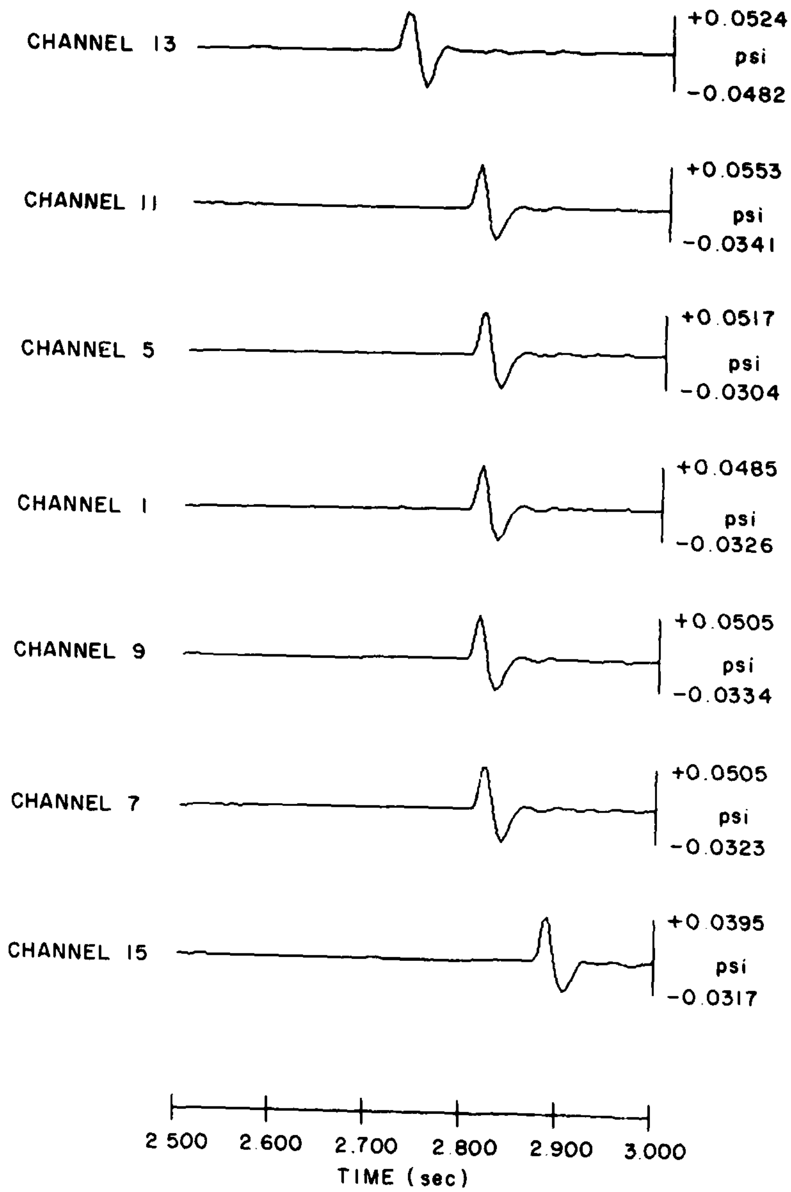


Figure B2. Acoustic Pulses Observed for EOD Range 2.3-kg Shots

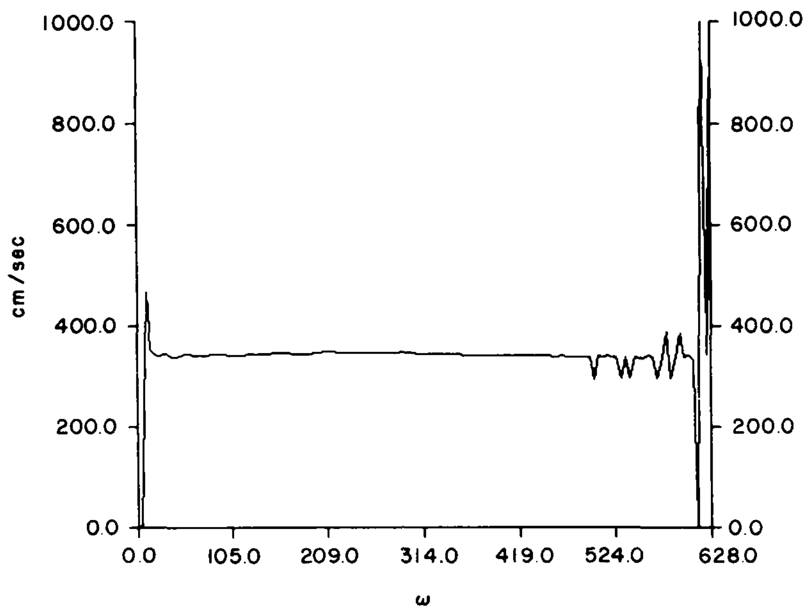


Figure B3. Phase Velocity Plot for EOD Range Shots

## List of Abbreviations and Acronyms

AB - Administration Building
AFGL - Air Force Geophysics Laboratory
cm - centimeter
dB - decibel(s)
DOF - degrees of freedom
EOD - Explosives and Ordnance Disposal
FE - finite element
ft - feet (0.305 m)
g - acceleration of gravity (980.6 $cm/sec^2$)
GDAS - Geophysical Data Acquisition System
GSS - Ground Support System
Hz - Hertz (unit of frequency)
kg - kilogram
KSC - Kennedy Space Center
LCC - Launch Control Center
LM - Launch Mount
m - meter(s)
MST - Mobile Service Tower
NASA - National Aeronautics and Space Administration
OASPL - Overall Sound Power Level
OFS - Orbiter Functional Simulator
PCR - Payload Changeout Room
PGHM - Payload Ground Handling Mechanism

| | |
|---|---|
| PPR | - Payload Preparation Room |
| PSD | - Power Spectral Density |
| psi | - pounds per square inch (6894.8 pascals) |
| SATAF | - Shuttle Activation Task Force |
| SD | - Space Division |
| sec | - second(s) |
| SRB | - Solid Rocket Booster |
| STS | - Space Transportation System |
| VAFB | - Vandenberg AFB |
| V23 | - The VAFB STS Launch Pad Complex |